Journal for ImmunoTherapy of Cancer

Salt-inducible kinase 3 protects tumor cells from cytotoxic T-cell attack by promoting TNF-induced NF-κB activation

Antonio Sorrentino ,[1,2] Ayse Nur Menevse ,[1] Tillmann Michels,[1,2] Valentina Volpin,[1,2] Franziska Christine Durst ,[1] Julian Sax,[1] Maria Xydia ,[1] Abir Hussein ,[1] Slava Stamova,[1] Steffen Spoerl,[1,3] Nicole Heuschneider,[1] Jasmin Muehlbauer,[1] Katharina Marlene Jeltsch,[1] Anchana Rathinasamy,[1] Melanie Werner-Klein,[1,4] Marco Breinig,[5,6,7] Damian Mikietyn,[1] Christian Kohler,[8] Isabel Poschke,[9,10,11] Sabrina Purr,[12] Olivia Reidell,[13] Catarina Martins Freire,[13] Rienk Offringa,[9] Claudia Gebhard,[1,14] Rainer Spang,[15] Michael Rehli,[1,14] Michael Boutros,[5] Christian Schmidl,[16] Nisit Khandelwal,[2,13] Philipp Beckhove [1,14]

To cite: Sorrentino A, Menevse AN, Michels T, *et al*. Salt-inducible kinase 3 protects tumor cells from cytotoxic T-cell attack by promoting TNF-induced NF-κB activation. *Journal for ImmunoTherapy of Cancer* 2022;**10**:e004258. doi:10.1136/jitc-2021-004258

► Additional supplemental material is published online only. To view, please visit the journal online (http://dx.doi.org/10.1136/jitc-2021-004258).

AS and ANM contributed equally.

Accepted 29 April 2022

For numbered affiliations see end of article.

Correspondence to
Dr Antonio Sorrentino; Antonio.Sorrentino88@outlook.com

Professor Philipp Beckhove; beckhove@rcii.de

ABSTRACT

Background Cancer immunotherapeutic strategies showed unprecedented results in the clinic. However, many patients do not respond to immuno-oncological treatments due to the occurrence of a plethora of immunological obstacles, including tumor intrinsic mechanisms of resistance to cytotoxic T-cell (TC) attack. Thus, a deeper understanding of these mechanisms is needed to develop successful immunotherapies.

Methods To identify novel genes that protect tumor cells from effective TC-mediated cytotoxicity, we performed a genetic screening in pancreatic cancer cells challenged with tumor-infiltrating lymphocytes and antigen-specific TCs.

Results The screening revealed 108 potential genes that protected tumor cells from TC attack. Among them, salt-inducible kinase 3 (SIK3) was one of the strongest hits identified in the screening. Both genetic and pharmacological inhibitions of SIK3 in tumor cells dramatically increased TC-mediated cytotoxicity in several in vitro coculture models, using different sources of tumor and TCs. Consistently, adoptive TC transfer of TILs led to tumor growth inhibition of SIK3-depleted cancer cells in vivo. Mechanistic analysis revealed that SIK3 rendered tumor cells susceptible to tumor necrosis factor (TNF) secreted by tumor-activated TCs. SIK3 promoted nuclear factor kappa B (NF-κB) nuclear translocation and inhibited caspase-8 and caspase-9 after TNF stimulation. Chromatin accessibility and transcriptome analyses showed that SIK3 knockdown profoundly impaired the expression of prosurvival genes under the TNF–NF-κB axis. TNF stimulation led to SIK3-dependent phosphorylation of the NF-κB upstream regulators inhibitory-κB kinase and NF-kappa-B inhibitor alpha on the one side, and to inhibition of histone deacetylase 4 on the other side, thus sustaining NF-κB activation and nuclear stabilization. A SIK3-dependent gene signature of TNF-mediated NF-κB activation was found in a majority of pancreatic cancers where it correlated with increased cytotoxic TC activity and poor prognosis.

Conclusion Our data reveal an abundant molecular mechanism that protects tumor cells from cytotoxic TC attack and demonstrate that pharmacological inhibition of this pathway is feasible.

WHAT IS ALREADY KNOWN ON THIS TOPIC

⇒ Tumor-intrinsic resistance to T cell (TC)-released cytokines, such as tumor necrosis factor (TNF)-α, has recently emerged as a major mechanism of tumor immune evasion. Yet, a deeper characterization of the genes that are responsible for this effect is needed.

WHAT THIS STUDY ADDS

⇒ Salt-inducible kinase 3 (SIK3) is a novel regulator of tumor-intrinsic resistance to cytotoxic TC attack.

⇒ SIK3 confers tumor cell protection from TC-released TNF by sustaining the expression of pro-survival and anti-apoptotic genes under the control of nuclear factor kappa B (NF-κB).

⇒ A TNF/SIK3/NF-κB-mediated gene signature correlated with significantly reduced patient survival in pancreatic cancer.

HOW THIS STUDY MIGHT AFFECT RESEARCH, PRACTICE AND/OR POLICY

⇒ Pharmacological inhibition of SIK3 might be an effective strategy to sensitize cancer cells to TC-based immunotherapies by rewiring tumor cell responses to TC-secreted TNF.

BACKGROUND

Immunotherapeutic strategies that enhance T-cell (TC) activation and cytotoxicity have shown significant clinical success in several cancer indications.[1] Nevertheless, a large

proportion of patients do not benefit from these interventions due to the occurrence of primary, adaptive, or acquired resistance to cancer immunotherapy (CIT).[2] Resistance mechanisms to CIT may have different origins, such as the onset of an immunosuppressive microenvironment that dampens the activity of immune cells against cancer.[3] Alternatively, tumor-intrinsic resistance mechanisms may render tumor cells invisible, or refractory to the attack of cytotoxic TCs.[4] Tumor-intrinsic unresponsiveness to TC-released perforin-granzyme B, Fas ligand, or proinflammatory cytokines, such as interferon-γ (IFN-γ) and tumor necrosis factor (TNF)-α, has recently emerged as a major mechanism of tumor immune evasion.[3 5–10] So far, therapeutic approaches have largely focused on targeting immune modulatory ligand–receptor interactions between tumor cells and TCs in order to increase cytotoxic TC function. However, successful tumor immune rejection might be as much determined by the tumor cells' individual response towards TC insult. Thus, a better understanding of the mechanisms that tumor cells exploit to evade the immune system is needed.

To address this, we conducted a genetic screening for genes that mediate tumor-intrinsic resistance to TC attack. We found that salt-inducible kinase 3 (SIK3) counteracts TC-mediated cytotoxicity by promoting TNF-induced nuclear factor kappa B (NF-κB) nuclear translocation and stabilization, leading to increased tumor cell survival and resistance against CIT. A TNF/SIK3/NF-κB-mediated gene signature was found in a vast majority of patients with pancreatic cancer with increased cytotoxic TC responses and correlated with significantly reduced patient survival. Thus, we reveal a novel molecular mechanism that protects tumor cells from cytotoxic TC attack.

METHODS

Cell lines

Human pancreatic ductal adenocarcinoma cell line PANC-1 (ATCC® CRL-1469™; source: male), human breast carcinoma cell line MCF7 (ATCC® HTB-22™, source: female), human embryonic kidney cell line HEK293T (ATCC® CRL-1573™, source: female) and colonic cancer cell line SW480 (ATCC® CCL-228™, source: male) were acquired from American Type Cell Culture (ATCC). PANC-1 and MCF7 were cultured under standard conditions in Dulbecco's Modified Eagle Medium (DMEM) media supplemented with 10% fetal calf serum, 100 U/ml penicillin G and 100 µg/ml streptomycin at 37 °C in a humidified atmosphere under 5% CO2. HEK293 and SW480 were cultured under standard conditions in Roswell Park Memorial Institute Medium (RPMI1640) media supplemented with 10% fetal calf serum, 100 U/ml penicillin G and 100 µg/ml streptomycin at 37 °C in a humidified atmosphere under 5% CO2. PANC-1-luc cells were generated after transfection with a pEGFP-luc plasmid (provided by Dr. Rudolf Haase, LMU Munich, Germany) and selected for the G418-resistance gene. TransIT (Mirus, Madison, USA) was used as transfection reagent according to the manufacturer's instructions. PANC-1 NF-κB reporter cells were generated using transfection with a pGL4.32 luc2/NF-κB-RE/hygro plasmid (Promega, Madison, USA), selection with hygromycin and serial dilution for clonal selection. Lipofectamin 3000 (Thermo Scientific) was used as transfection reagent according to the manufacturer's instruction.

Primary cell cultures

Primary melanoma M579 cells (isolated from an inguinal lymph node of a male patient with melanoma) were kindly provided by Professor Michal Lotem (Hadassah Hebrew University Medical Center, Israel) and cultured under standard conditions in complete melanoma media (60% DMEM, 20% RPMI1640, and 20% Ham's F12 Nutrient Mixture) supplemented with 10% fetal calf serum, 1% 4-(2-hydroxyethyl)-1-piperazineethanesulfonic acid (HEPES), 100 U/mL penicillin G and 100 µg/mL streptomycin at 37°C in a humidified atmosphere under 5% CO_2.

Tumor-infiltrating lymphocyte (TIL) isolation, expansion and culture

PANC-TIL and PANC-TIL2 were isolated from male patients with poorly differentiated pancreatic adenocarcinoma (PAAD) (PDAC) and enriched in $CD8^+$ TCs by flow cytometric cell sorting. TIL209 and TIL412 were isolated from inguinal lymph nodes of patients with melanoma and were kindly provided by Professor Michal Lotem (Hadassah Hebrew University Medical Center).Tumors were dissected and small pieces were cultured in 24-well tissue culture plates in complete lymphocyte media (CLM) with 6000 IU/mL interleukin (IL)-2 for 14 days.[11] The wells were checked for dense lymphocyte growth, and subsequently, the TILs were either frozen or expanded directly. Melanoma and PDAC-derived TILs were rapidly expanded using a modified version of the Rosenberg protocol.[11 12] TILs were thawed in RPMI medium with 10% human serum and 50 U/mL benzonase. Subsequently, they were incubated for 2 days (6×10^5 cells/mL in CLM with 6000 IU/mL IL-2) at 37°C and 5% CO_2. Mitotically inactivated feeder cells were generated from peripheral blood mononuclear cell buffy coats of healthy donors (three different donors) by irradiation with 60 Gy (Gamacell 1000). TILs were cocultured with feeder cells in a 1:100 ratio (eg, 2×10^6 TILs and 200×10^6 feeders) in 400 mL expansion medium (CLM/AIM-V 50/50) supplemented with 30 ng/mL OKT3 antibody and 3000 IU/mL IL-2 for 5 days without moving in a G-Rex 100 cell culture flask. Afterwards, 250 mL supernatant was replaced with 150 mL of fresh expansion medium supplemented with 3000 IU/mL IL-2 (for the complete 300 mL). On day 7, the TILs were resuspended in the medium and distributed into 3 G-Rex 100. One hundred fifty millilitres of AIM-V with 5% AB serum and 3000 IU/mL IL-2 (for the complete 250 mL) was added. On day 11, 150 mL of AIM-V with IL-2 was added to each flask. On the 14th day of rapid expansion, TILs were collected and counted.

TILs were frozen in aliquots of 20×10^6 in freezing media A (60% AB serum and 40% RPMI1640) and B (80% AB serum and 20% DMSO (Dimethyl sulfoxide).

After sufficient expansion TILs were aliquoted and cultured in CLM: RPMI1640, 10% human AB serum (Valley Biomedical), 1% HEPES, 100 U/mL penicillin G, 100 µg/mL streptomycin, and 0.01% beta-mercaptoethanol) supplemented with 3000 IU/mL IL-2 at 37°C in a humidified atmosphere under 5% CO_2 for 48 hours. Subsequently, TILs were deprived of IL-2 (CLM without IL-2) for 24 hours in the same setting before experiments.

Reverse small interfering RNA (siRNA) transfection

Briefly, for siRNA transfections, RNAiMAX (Thermo Scientific) was used. Two hundred microlitres of 250 nM siRNA solution was added to each well of a six-well plate. Four microlitres of RNAiMAX transfection reagent was diluted in 200 µL of RPMI (Merck Millipore) and incubated for 10 min at RT. Four hundred microlitres of RPMI was added, and 600 µL of RNAiMAX mix was given to the wells coated with siRNA and incubated for 30 min at RT. PANC-1 (2×10^5, wild type (WT) or PANC-1-luc), or 4×10^5 M579 cells were resuspended in 1.2 mL DMEM medium containing 10% FCS, seeded in the siRNA-RNAiMAX containing wells, and incubated for 72 hours at 37°C, 5% CO_2. For 96-well plate transfection, the aforementioned protocol was proportionally scaled down. All siRNAs were purchased from Dharmacon (Horizon). SIK3 siRNA deconvolution experiment was performed using siGENOME siRNA reagents–set of 4. The SIK3 siRNA sequence 1 was used for all other experiments.

Luciferase-based cytotoxicity assay

Tumor cells expressing the luciferase reporter gene were reverse transfected with the indicated siRNA. For the viability setting, only culture medium was added to tumor cells. For the cytotoxicity setting, either TILs, survivin-specific TCs, the supernatant of activated TILs (conditioned medium) or recombinant tumor necrosis factor (rHuTNF) was added to transfected tumor cells at desired effector to target (E:T) ratios or concentration and incubated for 20 hours at 37°C, 5% CO_2. After coculture, the supernatant was removed and the remaining tumor cells were lysed using 40 µL/well of cell lysis buffer for 10 min. Luciferase assay buffer (60 µL/well) was added and luciferase activity was measured using a microplate reader (TECAN, Männedorf, Switzerland). Luciferase activity is proportional to the amount of remaining live tumor cells. When indicated, raw data were normalized to negative controls. In some cases, data were shown as cytotoxicity:viability ratio. In this case, raw values were first normalized to negative control (siCtrl or DMSO) and then the ratio between the condition with TCs (cytotoxicity) versus condition with culture medium (viability) was calculated. Anti-epithelial cell adhesion molecule (EpCAM) x CD3 and anti-CD19 x CD3 bispecific antibodies (BsAbs) were generated at DKFZ by Dr. Gerd Moldenhauer.

RNAi screening

The primary RNAi screening was conducted as described,[13] using a sublibrary of the genome-wide siRNA library siGENOME (Dharmacon; GE Healthcare, Munich, Germany) comprising 2887 genes (online supplemental table S1).[8] In short, each well contained a pool of four non-overlapping siRNAs targeting the same gene. Positive and negative siRNA controls were added in each 384-well plate. Read-out was performed using the Mithras reader (Berthold, Bad Wildbad, Germany) with 0.1 s counting time. In addition to the luciferase-based primary screening, PANC-1 WT cells were reversed transfected with the siRNA library and an additional viability screening was conducted using the CellTiter-Glo (CTG) assay (Promega). Raw relative luminescence units from the primary screening were processed using the cellHTS2 package in R/Bioconductor. Values from both conditions were quantile normalized against each other using the aroma.light package in R. Differential scores (cytotoxicity vs viability) were calculated using the locally estimated scatterplot smoothing (LOESS) local regression fitting. To identify candidate hits, the following thresholds were applied on the −z-scores of the samples: for the viability setting, genes showing a −z of >2.0 or −z of <1.0 were excluded. For the cytotoxicity setting, programmed death ligand 1 (PD-L1) was used as threshold score. Additionally, genes having a score of >2.55 or <−1.55 in the CTG-based viability screening were filtered out from the candidate list. For the secondary screening, a customized library containing 155 selected siRNA pools from the primary screening was used in 96-well plates, and siRNA transfected tumor cells were in parallel challenged with TILs (E:T=25:1) and survivin-specific TCs (E:T=5:1).

In vivo experiments

Short hairpin (sh)Ctrl-M579 tumor cells were generated by viral transfection using NTS2 viral partcles (Mission PLKO.1 puro non-targeting shRNA High titer, SHC016H; Sigma). SIK3-specific shRNA (shSIK3)-M579 tumor cells were generated using SIK3 sh3 (clone: 37452-TRCN0000037452, target sequence: GCCAGGCT TTATCTTATCAAA; Sigma). Tumor cells were subjected to puromycin selection prior to usage. NOD/SCID gamma chain knockout (NSG) mice were subcutaneously injected with 3×10^5 shSIK3-M579 or shCtrl-M579 cells each into the right and left flanks of one mouse, respectively. After 3, 10, 17, and 24 days, mice received 1×10^6 TIL209 intravenously. Tumor volumes were determined using the following formula: tumor volume $(mm^2)=(width^2\times length)/(\pi/3)$.

TIL supernatants

TILs (1×10^6) were stimulated with 25 µL of Human T-Activator CD3/CD28 Dynabeads (Thermo Scientific), distributed in a 96-well plate (U-bottom) at 120 µL/well. Alternatively, 1.2×10^5 TILs were stimulated with 2.4×10^3 PANC-1 cells. After 24 hours of stimulation (polyclonal or tumor stimulation), plates were centrifuged at 450×g for

5 min and 100 µL/well of the supernatant was collected for cytokine detection or for further functional assays.

Functional neutralization and blocking assays

Anti-TNF (500 ng/ml; Abcam, anti-TRAIL (1 µg/ml; Abcam) anti-FASL (10 µg/ml; Biolegend) or respective isotype control monoclonal antibodies (mABs) (Abcam, Biolegend) were pre-incubated with the supernatant of activated TILs (polyclonal activation) for 1 h. Antibody-treated supernatants were used to stimulate siRNA transfected PANC-1-luc cells. For SIK inhibition 2 x 10^5 PANC-1-luc cells/well were incubated overnight in a 96 well plate. HG-9-91-01 was added at the indicated concentrations simultaneously with TILs (E:T = 50:1) or rHuTNF (final concentration:100 ng/ml; Prof. Daniela Männel, University of Regensburg). After 24h stimulation, luciferase-based cytotoxicity assay was performed. For blockade of TNFR-I, anti-TNFR-I mAb (20 µg/ml; Hycult biotech, Uden Netherland) or isotype control was incubated with rHuTNF (50 ng/ml) (for 1 h at 37 °C, 5% CO2. Antibody-treated rHuTNF media or control medium were used to stimulate PANC-1-luc cells for 24h before analysis.

RNA sequencing

PANC-1 cells were transfected either with Ctrl or SIK3-specific siRNA and treated with 100 ng/mL rHuTNF for up to 4 hours or left untreated. Afterwards, tumor cells were harvested using the RNeasy mini kit (Qiagen) according to the manufacturer's instructions. RNA from unstimulated siRNA-transfected tumor cells was used as negative control. RNA-seq libraries were generated using the ScriptSeq Complete Kit (Illumina, San Diego, USA) according to the manufacturer's instructions. Libraries were sequenced paired-end (2×75 bp) on a HiSeq 3000 at the BSF Biomedical Sequencing Facility (CeMM Research Center for Molecuar Medicine, Austrian Academy of Sciences, Vienna, Austria). Raw fastq data were quality controlled using FastQC (http://www.bioinformatics.babraham.ac.uk/projects/fastqc/) and mapped to the annotated GRCh38 assembly of the human genome using STAR V.2.5[14] and the following parameters: –alignSJoverhangMin 8 –alignSJDBoverhangMin 1 –alignMatesGapMax 1000000 –alignIntronMax 1 000 000, and –quantMode GeneCounts. Differentially expressed genes were analyzed using edgeR[15] and visualized using software packages in R. Gene set enrichment analyses were done using EnrichR.[16] RNA sequencing data have been deposited in the Gene Expression Omnibus (GEO) public functional genomic data repository under accession code GSE202305.

Assay for transposable-accessible chromatin with sequencing (ATAC-seq)

Chromatin accessibility mapping was performed using the ATAC-seq method as previously described,[17] with minor adaptations. Briefly, in each experiment, ~50 000 sorted cells were pelleted by centrifuging for 10 min at 4°C at 500×*g*. After centrifugation, the pellet was carefully lysed in 50 µL resuspension buffer supplemented with NP-40 (Sigma), Tween-20, and Digitonin (10 mM Tris–HCl pH 7.4, 10 mM NaCl, 3 mM $MgCl_2$, 0.1 % NP-40, 0.1% Tween-20, 0.01% Digitonin), and incubated for 3 min on ice. Then, 1 mL of ice-cold resuspension buffer supplemented with 0.1% Tween-20 was added, and the sample was centrifuged at 4°C at 500×*g* for 10 min. The supernatant was discarded, and the cell pellet was carefully resuspended in the transposition reaction (25 µL 2× TD buffer (Illumina), 2.5 µL TDE1 (Illumina), 16.5 µL phosphate-buffered saline (PBS), 5 µL nuclease-free water, 0.5 µL 1% Digitonin (Promega), and 0.5 µL 10% Tween-20 (Sigma)) for 30 min at 37°C on a shaker at 1000 rpm. Following DNA purification with the Clean and Concentrator-5 kit (Zymo) eluting in 23 µL, 2 µL of the eluted DNA was used in a quantitative 10 µL PCR reaction (1.25 µM forward and reverse custom Nextera primers,[17] 1× SYBR green final concentration) to estimate the optimum number of amplification cycles with the following programme: 72°C 5 min, 98°C 30 s, 25 cycles: 98°C 10 s, 63°C 30 s, 72°C 1 min; the final amplification of the library was carried out using the same PCR programme and the number of cycles according to the Cq value of the quantitative PCR (qPCR). Library amplification using custom Nextera primers was followed by solid-phase reversible immobilization (SPRI) size selection with AmpureXP beads to exclude fragments larger than 1200 bp. DNA concentration was measured with a Qubit fluorometer (Life Technologies). The libraries were sequenced using the Illumina NextSeq550 platform using a High Output Kit (75 cycles) in paired-end mode. ATAC-seq data have been deposited in the GEO public functional genomic data repository under accession code GSE202305.

TNF–SIK3–NF-κB-mediated gene expression index

Dataset: RNA-Sequencing data (RSEM values for 20 501 genes ranging from 0 to 10^6) from the second analysis pipeline (RNASeq V.2) for the PAAD cancer type together with matching clinical data was downloaded fromThe Cancer Genome Atlas (TCGA) Data Portal with the *TCGA2STAT* R package in V.1.2.[18] The original SIK3/TNF-mediated signature consists of 205 genes, but only 184 genes (90%) were available on the PAAD dataset. Only primary tumor samples were used for statistical analysis. A TNF/SIK3-mediated gene expression index was calculated as described further.

Quantification and statistical analysis

Statistical analyses were conducted using Prism software V.6.0 (GraphPad Software, La Jolla, California, USA). Results were reported as mean±SEM (SE of the mean) as indicated in the figure legends unless otherwise stated. We performed analyses of significance using Student's t-test assuming equal variance. Continuous biological variables were assumed to follow a normal distribution. A p value of <0.05 was considered to indicate statistical significance. All experiments with representative images

have been repeated at least twice and representative images are shown.

For statistical analysis of the TNF–SIK3–NF-κB-mediated gene expression index, an estimation of the extent of regulation of the SIK3/TNF-mediated signature on the PAAD profiles was performed by calculating a single representative value (index) for each sample from the signature consisting of 184 genes by fitting a standard additive model with independent gene and sample effects using Tukey's median polish procedure as previously described.[19 20] The survival probability was estimated by the Kaplan-Meier method, and differences were compared using the log-rank test. Both methods were applied as implemented in the R package *survminer* V.0.3.1.[21] The data matrix was scaled to standard units (z-scores) in order to make the expression values for selected genes comparable as the expression level of the genes varies.

RESULTS

High-throughput screening reveals multiple immune modulatory genes in human pancreatic cancer cells

To systematically identify genes that regulate tumor response towards TC attack, we adapted a high-throughput siRNA-based screening approach that was developed in our laboratory.[8 13] Due to its particular immune-resistant phenotype, we focused on pancreatic cancer. We targeted 2887 genes, including a broad spectrum of kinases, G-protein-coupled receptors (GPCRs) and other surface molecules (online supplemental table S1)[8] in PANC-1-luc cells using a siRNA library followed by coculture with patient-derived and HLA-matched tumor-infiltrating lymphocytes (PANC-TIL). PANC-TIL mainly consisted of $CD8^+$ TCs and showed an exhausted phenotype, as detected by expression of PD-1, LAG-3, and TIM-3 (figure 1A).[22] We observed modest killing activity on coculture of PANC-TIL with HLA-201^+ PANC-1 cells, but not with HLA-201^- ASPC1 cells (figure 1B). Blockade of major histocompatibility complex I (MHC-I) resulted in impaired cytotoxicity of PANC-TIL towards PANC-1 cells (online supplemental figure S1A), demonstrating that tumor cell killing occurred via T-cell receptor (TCR) engagement. Notably, MHC-I blockade did not completely abrogate tumor cell killing, suggesting that TCR-independent killing mechanisms may concomitantly occur in this coculture model. Additionally, PANC-TIL secreted IFN-γ on coculture with tumor cells (online supplemental figure S1B). The screen was run in the presence (cytotoxicity setting) or in the absence (viability setting) of cytotoxic TCs to exclude genes whose knockdown intrinsically affected cell viability. We detected >97% reduction of luciferase activity in PANC-1-luc cells after transfection with luciferase-specific siRNA, demonstrating efficient delivery of siRNAs in tumor cells (figure 1C). To identify positive controls for the viability setting, several known essential genes were knocked down in tumor cells.[23–26] Among them, transfection with siRNAs targeting ubiquitin C or a cocktail of siRNAs targeting multiple essential genes (siCD) strongly impaired tumor cell viability (figure 1C). To identify positive controls for the cytotoxicity setting, several tumor-associated immune modulators[27–29] were depleted in tumor cells using siRNAs. Of note, PD-L1 knockdown resulted in increased tumor cell death in the presence of cytotoxic TCs while having modest impact in the absence of TCs. PD-L1 knockdown was observed at both mRNA and protein levels (online supplemental figure S1C,D).

Robust technical performance of the screen was reflected in the high correlation scores between replicates (Pearson correlation: cytotoxicity readout=0.92, viability readout=0.90) as shown in figure 1E. Performance of the non-targeting control siRNAs, positive immune checkpoint control and positive viability control siRNAs, included on each screening plate, is also summarized in figure 1E. Altogether, these data confirmed the reliability and robustness of the screen. To identify genes with immune modulatory function, we excluded those hits whose knockdown markedly affected tumor cell viability per se as determined through a viability set-up (figure 1F). Genes were ranked according to their performance in the cytotoxicity versus viability readout, and only genes whose downregulation showed a stronger immune checkpoint phenotype than PD-L1 knockdown were selected (figure 1G). This procedure revealed 155 genes, among which IL17RA was already described as a tumor-associated immune modulatory receptor.[30] To confirm the immune modulatory potential of this primary hit list, we performed a secondary screen. In addition to PANC-TIL, we used antigen-specific TC clones recognizing the survivin protein (survivin TCs),[13] which is expressed by PANC-1 cells[31] (figure 1H). Immune modulatory activity against both the antigen-specific TC clone and patient-derived TILs was confirmed for 70% of the primary hits, resulting in 108 genes with potential immune regulatory function expressed by human pancreatic cancer. Overall, we detected a high correlation between the two TC sources (Pearson correlation=0.85)

SIK3 modulates intrinsic tumor resistance to cytotoxic TCs in several coculture models of human cancer

One of the genes showing the strongest phenotypes in the primary and secondary screen was SIK3 (figure 1F–H). SIK3 is a serine/threonine kinase involved in cell cycle progression and tumorigenesis and is overexpressed in several tumors such as breast, colorectal, and ovarian cancer.[32 33] Yet, its role in cancer immune evasion has not been addressed so far.

To validate on-target selectivity of SIK3-targeting siRNAs used for the screen, we transfected PANC-1-luc cells either with the three non-overlapping SIK3-specific siRNAs or with the siRNA pool used in the screen. Each of the single siRNA sequences induced an efficient SIK3 knockdown at both mRNA (online supplemental figure S2A) and protein (online supplemental figure S2B) levels, and reproduced the immune modulatory effect

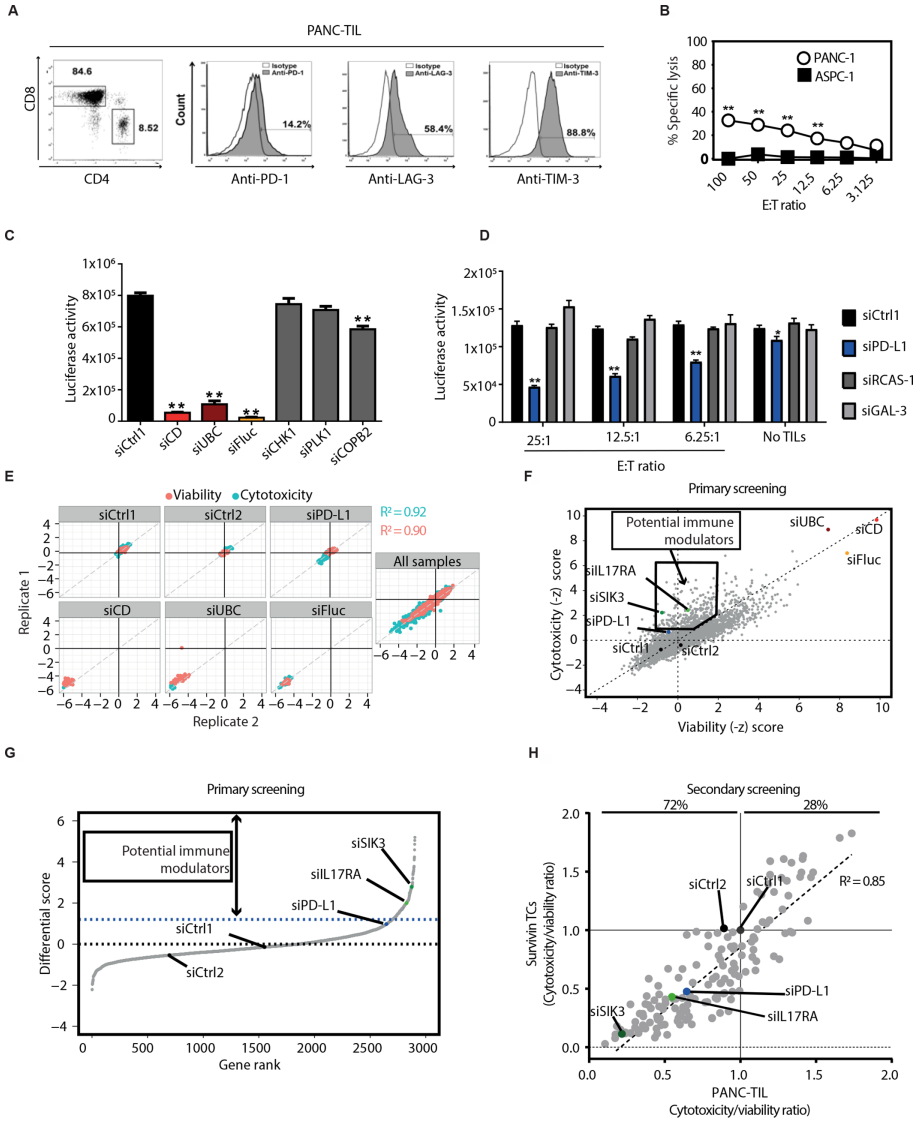

Figure 1 HT screening reveals multiple immune modulatory genes in human pancreatic cancer cells. (A) Characterization of PANC-TILs used for the primary HT screen. TILs were isolated from HLA-A201$^+$PDAC biopsies, enriched in CD8$^+$ subset and subjected to rapid expansion protocol. Left panel: CD4 and CD8 expression. Right panel: flow cytometry analysis for the exhaustion markers PD-1, LAG-3 and Tim-3 in CD3$^+$CD8$^+$ subpopulation. (B) Chromium release assay after 6-hour coculture of HLA-A201$^+$ PANC-1 or HLA-A201$^-$ ASPC-1 target cells with PANC-TIL using different E:T ratios. (C) Selection of viability controls (condition without PANC-TIL). PANC-1-luc cells were transfected with siRNA sequences, and luciferase-based cytotoxicity assay was performed (see the Methods section). (D) Selection of cytotoxicity controls. PANC-1-luc cells were transfected as in (C) with siRNA sequences targeting known immune modulators and subsequently cocultured with PANC-TIL at the indicated E:T ratios or culture medium. Luciferase-based cytotoxicity assay was performed. (E) Performance of viability and cytotoxicity controls in the primary HT screening. PANC-1 luciferase activity was measured in 384-well format after transfection with the siRNA library and the indicated control siRNA. Technical replicates were plotted against each other. Blue dots: cytotoxicity readout (with PANC-TIL), red dots: viability readout (without PANC-TIL). (F) Dot plot showing –z-scores of plate-normalized luciferase activity from transfected PANC-1-luc cells after coculture with TILs (cytotoxicity –z-score) or with culture medium (viability –z-score), using an siRNA library of 2887 genes plus controls. Cytotoxicity –z-score: influence of gene knockdown on TIL-mediated killing. Positive values: decreased cell viability. The black box shows genes which were considered as potential negative immune modulators. (G) Differential score between cytotoxicity and viability –z-scores using local regression (LOESS) rank. Genes with differential score higher than PD-L1 knockdown were selected. (H) Secondary screening using both PANC-TIL and antigen-specific surviving TCs. An siRNA library with the top 155 hits from the primary screening was used to transfect PANC-1-luc cells. Tumor cells were cocultured with indicated TC source for 20 hours and luciferase activity was measured. Cytotoxicity:viability ratio was calculated (see the Methods section). R^2 is the Pearson correlation of cytotoxicity:viability ratios between survivin-specific TCs and PANC-TIL-based screens. (A–D) Graphs show representative data of at least two independent experiments. (B–D) graphs show mean±SEM. P values were calculated using two-tailed Student t-test. *P<0.05, **P<0.01. E:T, effector to target; HT, high throughput; PDAC, pancreatic ductal adenocarcinoma; PD-L1, programmed death ligand 1; siCD, siRNAs targeting multiple essential genes; siFluc, luciferase-specific siRNA; siUBC, siRNA targeting ubiquitin C; TC, T cell; TIL, tumor-infiltrating lymphocyte.

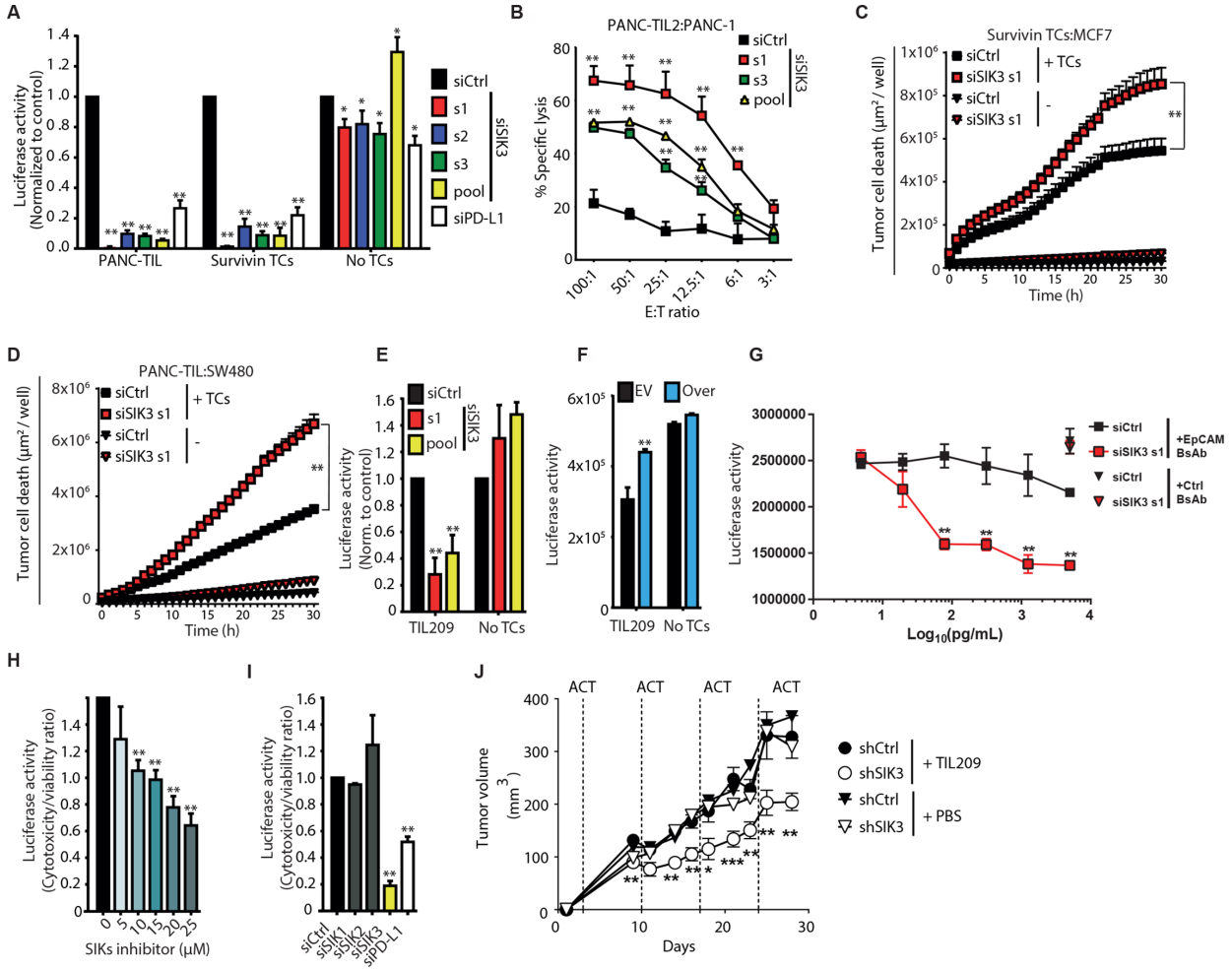

Figure 2 SIK3 inhibits TC-mediated killing across solid tumors. (A) Luciferase-based cytotoxicity assay using different siRNA sequences targeting SIK3 or controls. Data were normalized to siCtrl. (B) Chromium release assay for the detection of TC-mediated cytotoxicity of PANC-1 cells after 6-hour coculture with PANC-TIL2. (C,D) Real-time live cell microscopy for the evaluation of tumor cell death using YOYO-1 dye. Seventy-two hours after siRNA transfection, MCF-7 (C) and SW480 (D) were cocultured either with survivin TCs or with TILs, respectively. Graph shows the area of YOYO-1+ dead cells/well (µm²/well). (E) M579-luciferase expressing melanoma cells were transfected with indicated siRNAs and cocultured with HLA-201⁺-matched melanoma TILs. TC-mediated cytotoxicity was assessed as in (A). (F) M579 cells were transfected with SIK3 ORF (Over) or EV. TC-mediated cytotoxicity was assessed as in (A). Data were normalized to siCtrl1. (G) siSIK3 or siCtrl PANC-1-luc cells were cocultured with EpCAM×CD3 (EpCAM BsAb) or control CD19×CD3 (Ctrl BsAb) bispecific antibodies in the presence of CD8⁺ TCs from healthy donors. TC-mediated cytotoxicity was measured as in (A). (H) PANC-1-luc cells were cocultured with PANC-TIL in the presence of increasing concentrations of the pan-SIK inhibitor HG-9-91-01. TC-mediated cytotoxicity was measured as in (A). (I) Luciferase-based cytotoxicity assay of siRNA-transfected PANC-1-luc cells challenged with PANC-TIL after knockdown of SIK family member proteins or controls. Cytotoxicity:viability ratio was calculated (see the Methods section). (J) shCtrl or shSIK3 M579 melanoma cells were coengrafted subcutaneously in NSG mice subjected to ACT of TIL209 or PBS (n=9). Mean±SEM tumor volume. Statistical difference was calculated using unpaired Mann-Whitney U test. Data information: (A,E,H) cumulative data of three independent experiments and (B–D,F,G,I,J) representative data of at least two independent experiments. Columns show mean±SEM. P values were calculated using two-tailed Student t-test. *P<0.05, **P<0.01. E:T, effector to target; EV, empty vector; shSIK3, SIK3-specific shRNA; SIK3, salt-inducible kinase 3; TC, T cell; TIL, tumor-infiltrating lymphocyte.

observed in the screen (figure 2A). In accordance with the screening results, SIK3 silencing provided a stronger tumor lysis than PD-L1 depletion (online supplemental figure S2C) with no major effect on tumor cell viability in the absence of TCs. This was confirmed by another luciferase-independent assay (WST-1) of cell viability (online supplemental figure S2D).

Chromium release assay was conducted as a luciferase-independent standard test for specific TC lysis of PANC-1 cells after coculture with a different TIL derived from primary PDAC (PANC-TIL2) (figure 2B), which confirmed increased TIL-mediated killing of SIK3 knockdown tumor cells. SIK3 also regulated immune responsiveness in other cancer entities since its silencing in

breast (MCF-7) and colorectal (SW480) cancer cell lines caused a strong increase of tumor cell death after coculture with survivin-specific TCs or TILs, respectively (figure 2C,D). In a primary melanoma coculture model, abrogation of SIK3 potentiated TIL-mediated cytotoxicity (figure 2E), whereas overexpression of SIK3 dampened the cytotoxic potential of TIL209 (figure 2F). In addition to improving antigen-specific TC-mediated cytotoxicity, SIK3 knockdown also increased EpCAM×CD3 bispecific antibody-induced cytotoxicity (figure 2G).

In order to investigate a direct functional role of SIK3 kinase activity in cancer immune evasion, we treated TC–tumor cocultures with increasing concentrations of HG-9-91-01, an SIK family kinase inhibitor,[34] which recapitulated improved TIL-mediated killing in a dose-dependent manner (figure 2H). As this compound targets the family members SIK1 and SIK2 in addition to SIK3, we evaluated the individual impact of SIK isoforms in modulating TC-mediated cytotoxicity. However, knockdown of SIK1 and SIK2 did not improve TC-mediated killing compared with SIK3 knockdown (figure 2I). To confirm the role of SIK3 in mediating cancer resistance against immune attack in vivo, we stably knocked down SIK3 in human M579 tumor cells using shSIK3. We engrafted shSIK3 and WT cells into immune-deficient NSG mice and treated them by intravenous injections of TIL209. SIK3-proficient tumors were resistant against TIL209 treatment, while the growth of SIK3-deficient tumors was significantly delayed by TIL therapy (figure 2J).

SIK3 regulates tumor cell sensitivity to cytotoxic TC effector molecules

Cancer cells can exploit several mechanisms to evade immune-mediated destruction. These mechanisms may either dampen immune cell activity or decrease tumor sensitivity to effector molecules expressed by immune cells. SIK3 impairment in tumor cells did not improve TC activity, indicated by the production of effector molecules like IFN-γ, perforin or granzyme B in TC (online supplemental figure S3A-C). Hence, we hypothesized a role of SIK3 in mediating tumor cell resistance towards cytotoxic TC molecules. SIK3-depleted tumor cells were efficiently killed by the conditioned medium from activated TILs (Sup TILs), while their SIK3-proficient counterparts were resistant against this challenge (figure 3A,B). Of note, supernatant of unstimulated TCs did not alter tumor cell survival after SIK3 siRNA transfection (figure 3A). In line with its function as immune modulator, PD-L1 knockdown did not sensitize tumor cells towards TC effector molecules (figure 3B). Therefore, SIK3 is an intrinsic mediator of tumor cell resistance towards cytotoxic molecules released by activated TCs.

SIK3 regulates the response of tumor cells to TNF

To investigate whether SIK3 mediated the resistance against a distinct TC effector molecule, we blocked TNF, TRAIL, and FasL in the supernatant of activated TCs and assessed the response of SIK3-deficient tumor cells. Neutralization of TNF considerably diminished the cytotoxic potential of the TC supernatant on SIK3-depleted cells, while neutralization of FasL and TRAIL did not reduce tumor cell lysis in SIK3-deficient cells (figure 3C).

TNF is secreted by cytotoxic $CD8^+$ TC on TCR activation and is an important cytokine in cancer rejection by tumor-specific TCs.[35 36] Stimulation of TILs with tumor cells or anti-CD3/CD28 beads resulted in TNF production by $CD8^+$ TCs (figure 3D,E). On TNF neutralization, we observed a complete rescue of TC-induced tumor cell death in SIK3-depleted cells (figure 3F). The same treatment in control tumor cells did not alter cell viability in comparison to isotype control (online supplemental figure S3D). Treatment with rHuTNF was sufficient to induce tumor cell lysis of SIK3-deficient tumor cells, while the same treatment triggered slight tumor proliferation of SIK3-proficient (siCtrl) tumor cells (figure 3G). Real-time live-cell microscopy revealed massive cell death of SIK3-depleted PANC-1 cells within the first 6 hours of TNF treatment (figure 3H and online supplemental video 1). These observations were also confirmed in MCF-7 breast cancer cells (online supplemental figure S3E). Blockade of SIK-3 kinase with HG-9-91-01 enhanced tumor cell cytotoxicity on TNF stimulation (figure 3I). To assess the relevance of SIK3 for protection against TNF-mediated cytotoxicity, we investigated whether SIK3 inhibition by HG-9-91-01 improved tumor cell destruction after rHuTNF treatment in 94 human cancer cell lines covering a broad variety of different tumor entities. Forty-seven cell lines showed increased tumor cell destruction on SIK3 inhibition (online supplemental figure S3F and online supplemental table S2).

TNF mediates its biological effects by binding to two distinct receptors: TNFR-I and TNFR-II.[37 38] PANC-1 cells expressed TNFR-I but not TNFR-II (online supplemental figure S3G). TNFR-I blockade in SIK3-depleted tumor cells abrogated TNF-induced cytotoxicity (figure 3J) but did not significantly alter tumor cell viability in siCtrl-transfected PANC-1 cells (online supplemental figure S3H). These data demonstrate that SIK3 determines the fate of tumor cells after TNFR-I stimulation.

SIK3 prevents TNF-induced apoptosis by modulating NF-κB nuclear translocation and chromatin accessibility

TNFR-I activation induces multiple downstream signaling events such as apoptosis via caspase cleavage but also activation of prosurvival transcription factors such as NF-κB.[39] We observed increased cleavage of both caspase-8 and caspase-9 after SIK3 depletion in tumor cells following rHuTNF treatment (figure 4A,B). SIK3-depleted cells showed increased levels of phosphorylated c-Jun N-terminal protein kinase (figure 4C). JNK phosphorylation occurs on TNF stimulation and mediates apoptosis in the absence of activated NF-κB,[40] which is a potent negative regulator of TNF-induced apoptosis.[41 42] On the contrary, SIK3 overexpression resulted in increased NF-κB nuclear translocation as detected by ELISA of nuclear lysates from PANC-1 cells (figure 4D). Furthermore, SIK3 knockdown

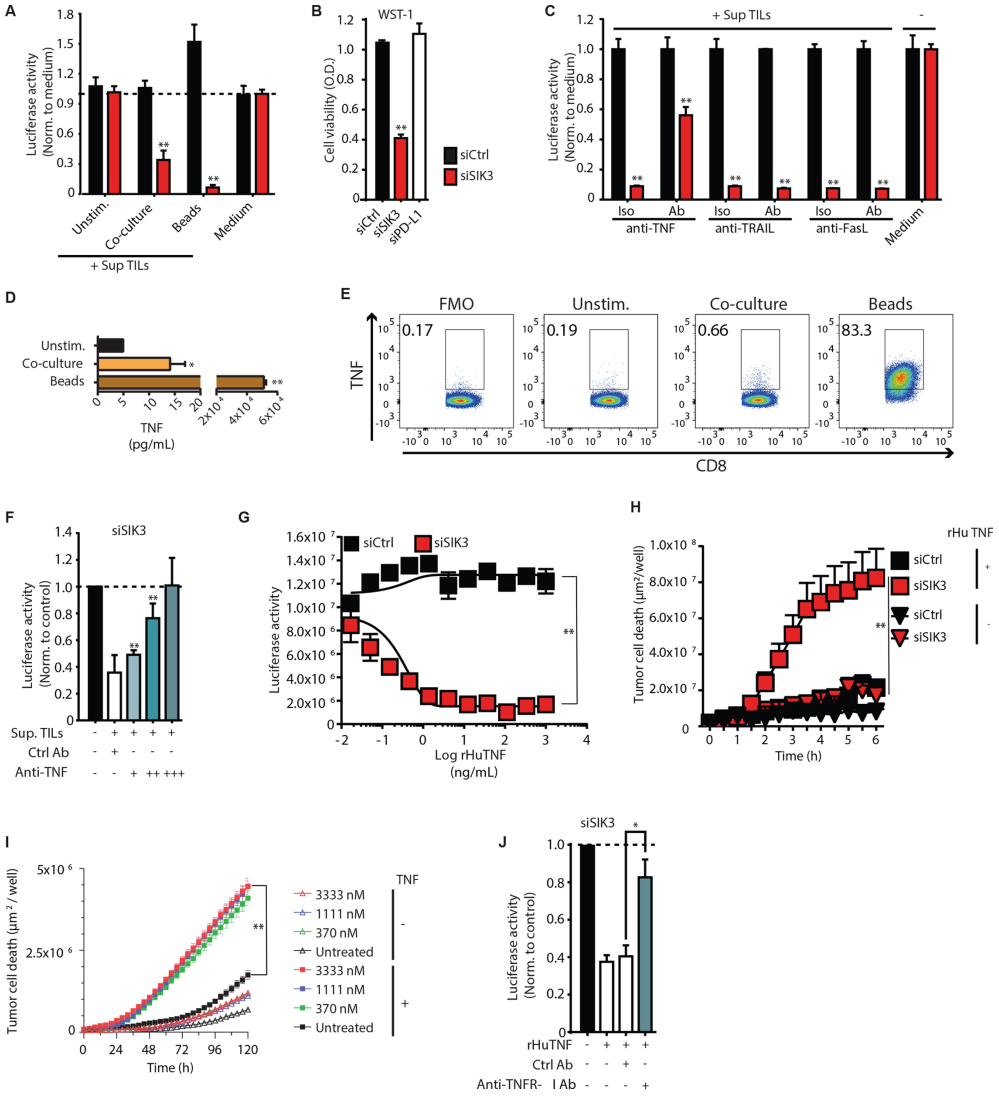

Figure 3 SIK3 mediates resistance to TNF secreted by activated TCs. (A) SIK3 depletion sensitizes tumor cells to conditioned media from activated TCs. PANC-1-luc cells were transfected with the indicated siRNAs. After 72 hours, cells were treated with the supernatant of unstimulated, tumor-activated or polyclonally activated TILs (by anti-CD3/CD28 beads), and tumor cell survival was determined by analysis of luciferase activity. (B). WST-1 assay for the assessment of cell viability of siRNA-transfected PANC-1 cells after challenge with the conditioned of polyclonally activated TILs. (C) Identification of TC effector molecules upstream of SIK3. PANC-1-luc cells were transfected with indicated siRNAs for 72 hours and subjected to the supernatant of polyclonally activated TILs. Stimulation was conducted in the presence of anti-TNF, anti-TRAIL or anti-FasL Ab or Iso controls. luciferase-based cytotoxicity assay was conducted to determine cytotoxicity of tumor cells on the indicated treatment. (D) Luminex assay for the detection of secreted TNF from PANC-TIL. TILs were cocultured either with PANC-1 cells or polyclonally stimulated. Unstimulated TILs were used as negative control. (E) Catch assay for the detection of TNF-secreting $CD8^+$ TCs from TILs. TCs were stimulated either with PANC-1 cells or with anti-CD3/CD28 beads for 12 hours. Unstimulated TILs were used as negative control. (F) TNF neutralization rescues siSIK3 tumor cells from conditioned medium-induced cytotoxicity. Supernatant from polyclonally stimulated TCs was incubated with 100 (+), 300 (++) or 900 (+++) ng/mL of anti-TNF neutralizing Ab. Iso control (Ctrl AB) was used at a concentration of 900 ng/mL. Afterwards, siSIK3 transfected PANC-1-luc cells were subjected to the pretreated supernatant for 24 hours and cytotoxicity was measured using luciferase-based cytotoxicity assay. Data normalized to siCtrl. (G). Dose–response effect of rHuTNF treatment on the viability of siRNA transfected PANC-1-luc cells. Tumor cells were stimulated with indicated concentrations of rHuTNF for 24 hours, and cytotoxicity was measured by analysis of luciferase activity. (H) Effect of 100 ng/mL TNF treatment on the viability of transfected PANC-1 cells. Cell death was evaluated using real-time live cell microscopy, measuring the nuclear incorporation of YOYO-1 dye. The graph shows the area of YOYO-1+ cells/well (μm^2/well). (I) Effect of pharmacological SIK3 inhibition on TNF-induced apoptosis of PANC-1 cells. PANC-1 cells were treated with different concentrations of HG-9-91-01 before the addition of 100 ng/mL rHuTNF for 120 hours. Cell death was evaluated as in (I). (J) Effect of TNFR-I blockade on siSIK3 transfected PANC-1-luc cells after treatment with the 100 ng/mL of rHuTNF. Luciferase intensity was measured as in (F). Data information: representative data of at least two independent experiments. Columns show mean±SEM. P values were calculated using two-tailed Student t-test. *P<0.05, **P<0.01. Ab, antibody; Iso, isotype; rHuTNF, recombinant tumor necrosis factor; SIK3, salt-inducible kinase 3; TC, T cell; TIL, tumor-infiltrating lymphocyte; TNF, tumor necrosis factor; TRAIL, tumor necrosis factor-related apoptosis-inducing ligand.

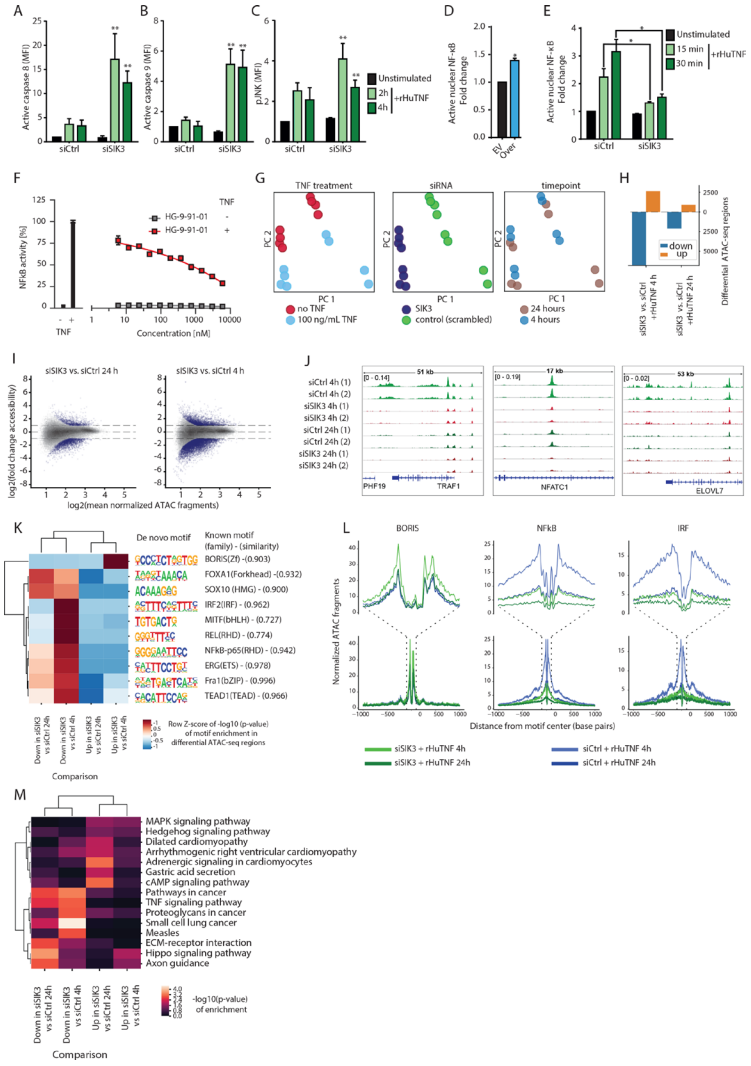

Figure 4 SIK3 prevents TNF-induced apoptosis via NF-κB activation. (A–C) siRNA-transfected PANC-1-luc cells were treated with 100 ng/mL of rHuTNF. At the indicated time points, tumor cells were harvested and total protein fraction was isolated. Luminex assay was performed for active caspase 8 (A), active caspase 9 (B), and pJNK (C). Graphs show MFI of analyte-specific beads after normalization to Glyceraldehyde-3-phosphate dehydrogenase (GAPDH). (D) PANC-1 cells were transiently transfected either with SIK3 overexpressing vector (Over) or with control vector (EV) for 48 hours. Afterwards, ELISA was performed for detection of nuclear p65 subunit of NF-κB. (E) PANC-1 cells were transfected with indicated siRNAs for 72 hours and treated with 100 ng/mL rHuTNF or culture medium for the indicated time points. p65 NF-κB ELISA was conducted as in (D). (F) Effect of pharmacological SIK3 inhibition on NF-κB activity. PANC-1 cells expressed luciferase under the control of an NF-κB promoter. Reporter PANC-1 were treated with different concentrations of HG-9-91-01 before the addition of 10 ng/mL rHuTNF for 8 hours. Cells were lysed and luciferase activity was measured. Data are shown as percent of NF-κB activity normalized to PANC-1 cells treated with 10 ng/mL rHuTNF without inhibitor. (G) Principal component analysis based on all identified chromatin accessible sites over all samples comprising siRNA transfected PANC-1-luc cells that were either untreated or treated with 100 ng/mL of rHuTNF for 4 hour or 24 hours. (H) Numbers of significant differentially accessible regions between comparison of SIK3 knockout and WT PANC-1 cells treated with rHuTNF for 4 or 24 hours (Benjamini-Hochberg corrected padj <0.05, $\log_2$ fold change >1, normalized mean accessibility ≥10). (I) M (log ratio) and A (average) (MA)-plot showing the $\log_2$ fold change and mean accessibility in the comparisons from (H). Significant differentially accessible regions are colored in dark violet. (J) Representative IGV genome browser snapshots of the TRAF1 locus for SIK3 knockdown and WT PANC-1 cells treated with rHuTNF for 4 or 24 hours. (K) Motif analysis of individual comparisons from (H). color code of heatmap indicates significance (z-score of $\log_{10}$ p value) of de novo identified transcription factor motifs in differential peaks from the respective pairwise comparisons. (L) ATAC-seq signal at motif-centered peaks containing the de novo discovered motifs of BORIS, NF-κB, and IRF from (K). X-axis shows distance from motif center in bp, y-axis number of normalized reads. (M) Kyoto Encyclopedia of Genes and Genomes (KEGG) pathway enrichment of genes in the vicinity of differential accessible chromatin regions from comparisons in (H). (A–C,E) Cumulative data of three independent experiments. (D,F) Representative data of at least two independent experiments. Columns show mean±SEM. P values were calculated using two-tailed Student t-test. *P<0.05, **P<0.01. ATAC-seq, assay for transposable-accessible chromatin with sequencing; bp, base pair; EV, empty vector; IRF, interferon regulatory factor; MFI, median fluorescent intensity; NF-κB, nuclear factor kappa B; pJNK, c-Jun N-terminal protein kinase; rHuTNF, recombinant tumor necrosis factor; SIK3, salt-inducible kinase 3; TNF, tumor necrosis factor; WT, wild type.

or functional inhibition led to a dramatic reduction of NF-κB activation on rHuTNF stimulation (figure 4E,F). Coculture of PANC-1 cells carrying a reporter gene for NF-κB activation with antigen-specific TCs confirmed that TC-induced NF-κB activation was regulated by SIK3 (online supplemental figure S4A). Taken together, these data demonstrate that SIK3 modulates resistance to apoptosis by promoting NF-κB nuclear translocation and stabilization after TNFR-I activation in tumor cells.

To better understand the role of SIK3 in TNF signaling, we determined the effect of TNFR-I stimulation on the chromatin landscape in SIK3-proficient and SIK3-deficient PANC-1 cells using the assay of transposase accessible chromatin (ATAC-seq). PANC-1 (siCtrl) treatment with 100 ng/mL rHuTNF resulted in remarkable changes in chromatin accessibility genome-wide, while SIK3 knockdown strongly impacted the molecular response of PANC-1 cells to TNF (figure 4G). On 4-hour of stimulation with rHuTNF, SIK3 silencing resulted in differential loss of more than 6000 and gain of more than 2500 open chromatin regions, respectively (figure 4H,I). Among the genetic loci depending on SIK3 activity, we identified regions critical for tumor cell initiation, progression, invasion, apoptosis resistance, and proliferation of pancreatic cancer, such as NFATC1,[43–46] TRAF1,[47] or ELOVL7[48] (figure 4J). De novo motif analysis within differentially accessible chromatin regions revealed enrichment of several transcription factor-binding sites (figure 4K). Notably, SIK3 knockdown caused a massive loss of accessible chromatin signal at NF-κB and interferon regulatory factors (IRFs) consensus binding sites (figure 4L). Finally, differentially accessible sites were located near genes involved in multiple related tumorigenic pathways, including a loss of TNF signaling (figure 4M). These data demonstrated a central role of SIK3 in modulating chromatin accessibility of tumor cells on TNF stimulation—likely in an indirect manner—by modulating transcription factors from the NF-κB, IRF and other TF families.

SIK3 sustains the expression of NF-κB target genes after TNF treatment

To extend these data, we performed transcriptome analyses in control or SIK3-depleted PANC-1 cells with or without rHuTNF treatment. SIK3 knockdown altered gene expression to some degree in the absence of TNF stimulation (online supplemental figure S4B–D). However, after 4 hours of rHuTNF treatment, a marked reduced transcription of NF-κB target genes was the most pronounced alteration in SIK3-depleted cells (figure 5A). Among the differentially expressed genes, several canonical antiapoptotic and prosurvival genes were further analyzed in more detail, both at RNA and protein levels. Expression of TNF-α induced protein 3 (A20),[49 50] inhibitor of apoptosis 2 (cIAP2),[51 52] and FLICE-like inhibitory protein (cFLIP)[53] was strongly enhanced by TNF treatment in siCtrl cells, whereas SIK3-deficient cells showed reduced expression of those genes at baseline and impaired upregulation on TNF treatment. Myeloid leukemia cell differentiation protein (MCL1),[54 55] and X-linked inhibitor of apoptosis protein (XIAP)[56] RNA and protein expressions did not increase on TNF treatment in siCtrl cells, yet expression levels were remarkably lower in siSIK3 transfected cells both at baseline and on TNF treatment as compared with siCtrl (RNAseq, online supplemental figure S4E; qPCR, figure 5B; and western blot (WB), figure 5C). Taken together, these data indicated that SIK3 protected tumor cells from TNF-induced apoptosis by upregulating several proapoptotic and prosurvival genes under the control of NF-κB. To investigate whether any of these target gene conferred resistance to TNF treatment in the absence of SIK3, we stably upregulated them in PANC-1 cells and subsequently silenced SIK3. Successful gene overexpression was confirmed both at RNA and protein level (online supplemental figure S4F,G). Luciferase-based cytotoxicity assay showed that overexpression of cFLIP, XIAP, and MCL1 partially protected tumor cells from TNF-mediated cytotoxicity in SIK3-depleted cells, whereas overexpression of cIAP2 did not show significant rescue in the same experiment. Coherent with its role as negative regulator of the NF-κB signaling, overexpression of A20 exacerbated the cytotoxic effect of TNF in SIK3-depleted cells (figure 5D).[57–60] Notably, none of the tested genes led to complete rescue from TNF-induced cytotoxicity on overexpression, indicating that upregulation of a single gene in the TNF–SIK3–NF-κB pathway may not be sufficient to protect SIK3-depleted tumor cells from TNF-induced cytotoxicity.

Integration of data from RNA-seq and ATAC-seq revealed a large overlap of differentially SIK3-regulated open chromatin regions and differentially expressed genes (figure 5E). Among them, multiple genes activated by SIK3 have been linked with tumor-promoting functions (online supplemental table S3), while genes associated with tumor suppression were largely repressed by SIK3 (online supplemental table S4). Taken together, these data demonstrated a pivotal role of SIK3 in regulating the ability of NF-κB in inducing its target genes on TNF stimulation.

SIK3 promotes NF-κB activation via inhibitory-κB kinase (IKK)α/β/NF-kappa-B inhibitor alpha (IκBα) phosphorylation and its nuclear retention via histone deacetylase 4 (HDAC4) inhibition

Based on these observations, we hypothesized a role of TNF in activating SIK3 via its upstream regulator, the liver kinase B1 (LKB1).[61 62] We found that treatment of PANC-1 cells with rHuTNF induced only modest phosphorylation of LKB1 (figure 6A). Next, we knocked down LKB1 in PANC-1 cells and subjected them to TNF treatment. LKB1 knockdown efficiency was successfully confirmed at the mRNA level (online supplemental figure S5A). In contrast to SIK3 knockdown, downregulation of LKB1 did not improve TNF-mediated cytotoxicity of PANC-1 cells (online supplemental figure S5B). Additionally, LKB1 downregulation did not impair, but rather improved NF-κB activation in TNF-treated PANC-1 cells (online supplemental figure S5C). Taken together, these data did not confirm the existence of a TNF–LKB1–SIK3 axis in this tumor model.

Next we sought to investigate the mechanism by which SIK3 regulates NF-κB activation. Canonically, TNF

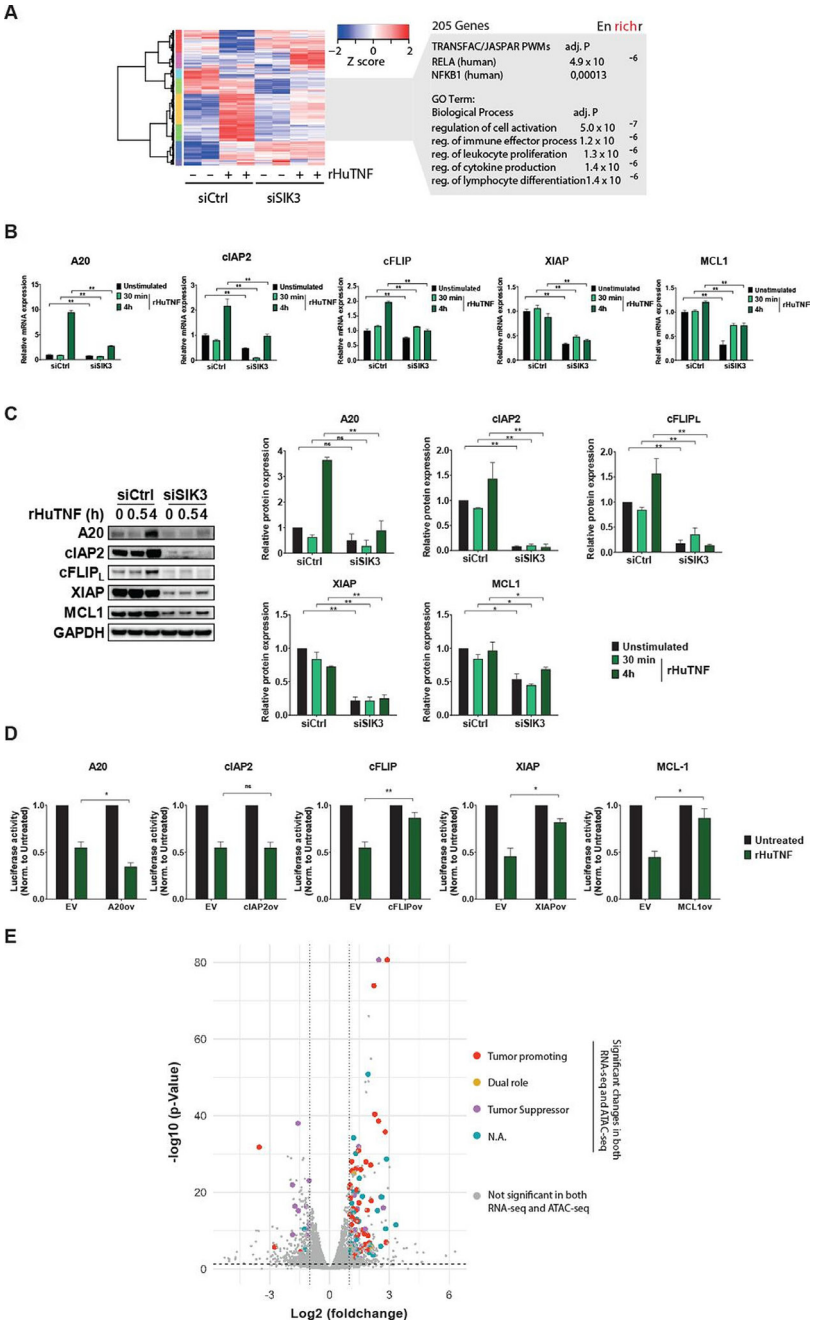

Figure 5 SIK3 sustains tumor-promoting gene signature after TNF stimulation (A) Two-dimensional hierarchical clustering of 386 genes that were significantly regulated by TNF after 4 hours and significantly affected by SIK3 knockdown. The right panel shows representative gene enrichment analysis for genes having reduced or missing induction by TNF after SIK3 knockdown (fold change ≥2, normalized counts per million >2, false discovery rate (FDR) ≤0.05). (B) qPCR for the detection of NF-κB target genes on 100 ng/mL rHuTNF treatment and SIK3 knockdown in PANC-1 cells. Data were normalized to GAPDH. (C) Assessment of protein expression of NF-κB target genes on 100 ng/mL rHuTNF treatment and SIK3 knockdown in PANC-1 cells. Left panel: representative WB experiment, right panel: relative quantification of protein expression normalized to GAPDH. (D) Luciferase-based cytotoxicity assay for the impact of the overexpression of NF-κB target genes in SIK3 knockout PANC-1 cells. Overespression was performed as described in online supplemental material and methods. Afterwards, cells were transfected with SIK3 siRNA for 72 hours and subsequently subjected to 100 ng/mL rHuTNF for 24 hours. (E) Volcano plot showing differentially expressed genes (from RNA-seq, rHuTNF treatment in siCtrl vs siSIK3 cells) that also have a significant differentially accessible region (determined by ATAC-seq) in their vicinity are highlighted and colored due to their role in tumor biology (see also online supplemental tables S3 and S4).(B) Representative data of at least two independent experiments. (C) Cumulative data of two independent experiments. (D) Cumulative data of at least three different experiments. WB quantifications were obtained by combining two independent experiments. Columns show mean±SEM. P values were calculated using two-tailed Student' t-test. *P<0.05, **P<0.01. ATAC-seq, assay for transposable-accessible chromatin with sequencing; EV, empty vector; NF-κB, nuclear factor kappa B; ns, not significant; rHuTNF, recombinant tumor necrosis factor; SIK3, salt-inducible kinase 3; TNF, tumor necrosis factor.

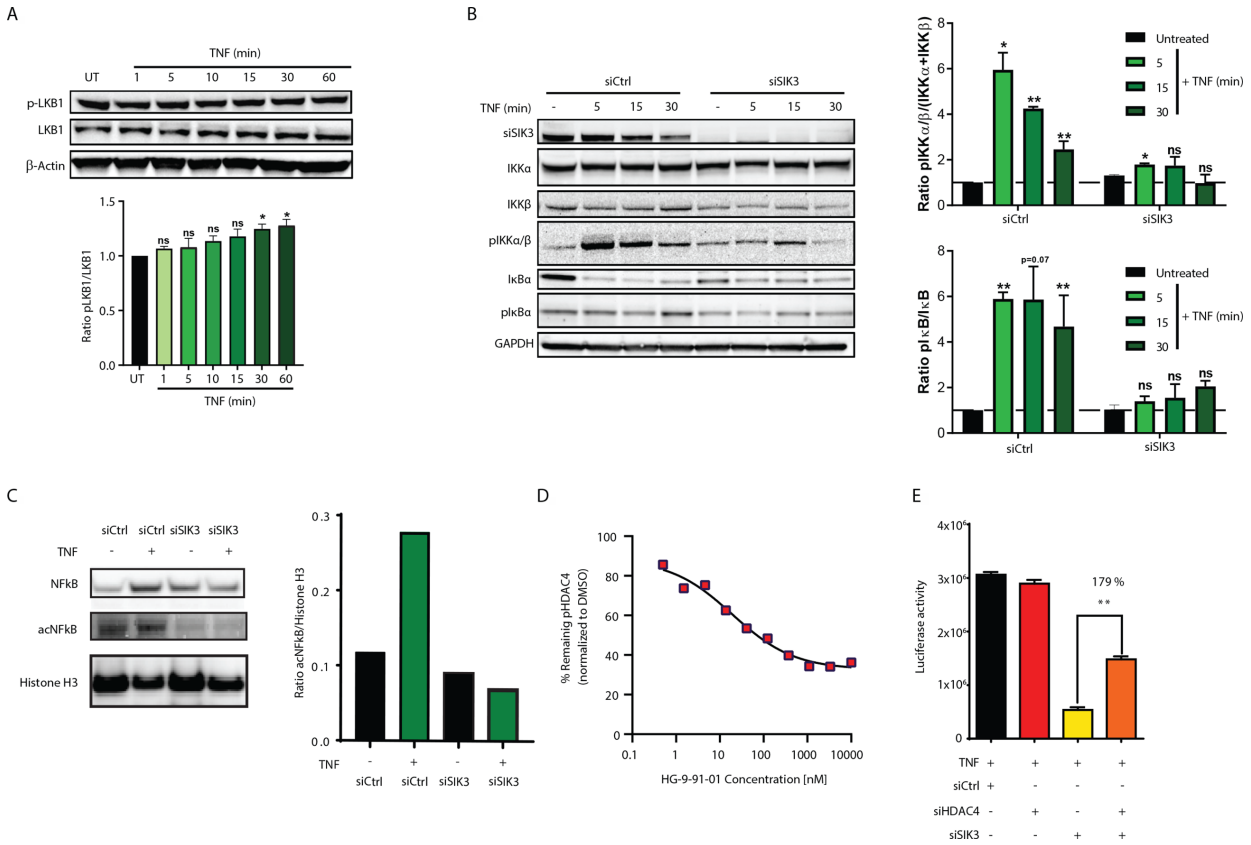

Figure 6 Mechanisms of TNF-induced NF-κB activation by SIK3. (A) Upper panel: immunoblot analysis of pLKB1, LKB1 and β-actin (loading control) in PANC-1 wild-type cells UT or stimulated for 1–60 min with TNF. Lower panel: quantification of pLKB1 expression normalized to total LKB1. (B) Left panel: immunoblot analysis of upstream regulators of NF-κB. Right panel: quantification of pIKKα/β expression normalized to total IKKα+IKKβ and quantification of pIκBα normalized to total pIκBα. (C) Left panel: immunoblot analysis of NF-κB, acNF-κB and histone H3 (nuclear loading control). Right panel: quantification of nuclear acNF-κB expression normalized to nuclear histone H3 expression. (D). Effect of pharmacological SIK3 inhibition on HDAC4 phosphorylation. PANC-1 cells were treated with different concentrations of HG-9-91-01 for 3 hours in the presence of 10 ng/mL rHuTNF. Whole cell lysates were analyzed in an meso scale discovery (MSD) assay with anti-HDAC4 capture and anti-pHDAC4 detection antibodies. Data are shown as percent of HDAC4 phosphorylation normalized to UT PANC-1 (DMSO only). (E) HDAC4 knockdown rescues siSIK3 PANC-1 cells from TNF-induced cytotoxicity. TNF-induced killing of PANC-1-luc cells determined by the luciferase activity of remaining tumor cells. PANC-1-luc cells were transfected with indicated siRNAs for 72 hours and stimulated with 100 ng/mL of rHuTNF for 24 hours. (A–E) Representative data of two independent experiments. WB quantifications were obtained by combining two independent experiments. Columns show mean±SEM. P values were calculated using two-tailed Student t-test. *P<0.05, **P<0.01. acNF-κB, acetylated NF-κB; HDAC4, histone deacetylase 4; IKK, inhibitory-κB kinase; LKB1, liver kinase B1; NF-κB, nuclear factor kappa B; pLKB1, phosphorylated LKB1; SIK3, salt-inducible kinase 3; TNF, tumor necrosis factor; UT, untreated.

activates NF-κB via IKKα and IKKβ phosphorylation that induces IκBα phosphorylation and its subsequent degradation.[63 64] Coherently, TNF treatment induced phosphorylation of IKK proteins within 5 min from the stimulus in PANC-1 cells (figure 6B). Additionally, reduced levels of total IκB and relative increased levels of pIκB were observed. Strikingly, SIK3-depleted tumor cells showed marked impairment of IKKα/β and IκB protein phosphorylation (figure 6B). These data indicate a role of SIK3 in promoting the upstream signaling cascade of TNF-induced NF-κB activation by sustaining, likely indirectly, IKKα/β protein phosphorylation.

Acetylation of NF-κB is a post-translational modification that stabilizes NF-κB nuclear retention and gene expression.[65 66] Consistently, we observed increased acetylated NF-κB (acNF-κB) on rHuTNF stimulation in SIK3-proficient cells (siCtrl). However, SIK3-deficient cells failed to increase acNF-κB after rHuTNF treatment (figure 6C). Among the regulators of NF-κB acetylation, HDAC4 decreases NF-κB activation by deacetylating the NF-κB p65 subunit.[62 67] Notably, SIK3 phosphorylates HDAC4 and inhibits its activity.[62] We confirmed that HDAC4 is negatively regulated by SIK3, as phosphorylation of HDAC4 was abrogated by the SIK3 inhibitor HG-9-91-01 (figure 6D). Therefore, we hypothesized that SIK3 increases NF-κB acetylation and nuclear stabilization by inhibiting HDAC4 protein levels. To prove this hypothesis, we silenced HDAC4 in SIK3-depleted tumor cells and evaluated tumor cell cytotoxicity after rHuTNF treatment. Indeed, SIK3/HDAC4 double-deficient PANC-1 cells showed decreased TNF-induced cytotoxicity compared with tumor cells transfected with SIK3-specific siRNA

alone (figure 6E). Thus, on TNF stimulation, SIK3 stabilizes NF-κB activation, at least partially, through NF-κB acetylation and HDAC4 inhibition. Taken together, these data indicate a dual role of SIK3 in promoting NF-κB signaling by both positively modulating its upstream regulators and concomitantly inhibiting its nuclear repressors.

TNF/SIK3-inducible gene expression signature is associated with poor prognosis in patients with pancreatic cancer

Comparative transcriptome analysis of TNF-stimulated SIK3-proficient and SIK3-deficient cells revealed altogether 386 genes that were significantly regulated by SIK3 after TNF stimulation (figure 5A) in pancreatic tumor cells. Among those, 205 genes were attributable to NF-κB activation. We investigated the expression of these genes in the PAAD dataset of the TCGA. One hundred eighty-four of the genes were also covered in this dataset and were condensed to a single index per patient as previously described,[20] yielding to quantitative NF-κB indices for 178 patients with primary PAAD. The majority of patients showed high index expression (figure 7A, blue dots), whereas a smaller group of patients showed impaired signature expression (figure 7A, red dots). Notably, the deficiency in TNF/SIK3-inducible NF-κB gene signature expression correlated with improved survival (p=0.0012). More than 75% of patients with low index were still alive after 7 years, while the median overall survival in the index high group was less than 2 years (p=0.0012) (figure 7B).

A high index significantly correlated not only with increased expression of SIK3 and TNF but also particularly with increased CD8$^+$ TC infiltration and cytotoxic TC activity, as determined by granzyme B and perforin expression (figure 7C–F). This indicates a direct link

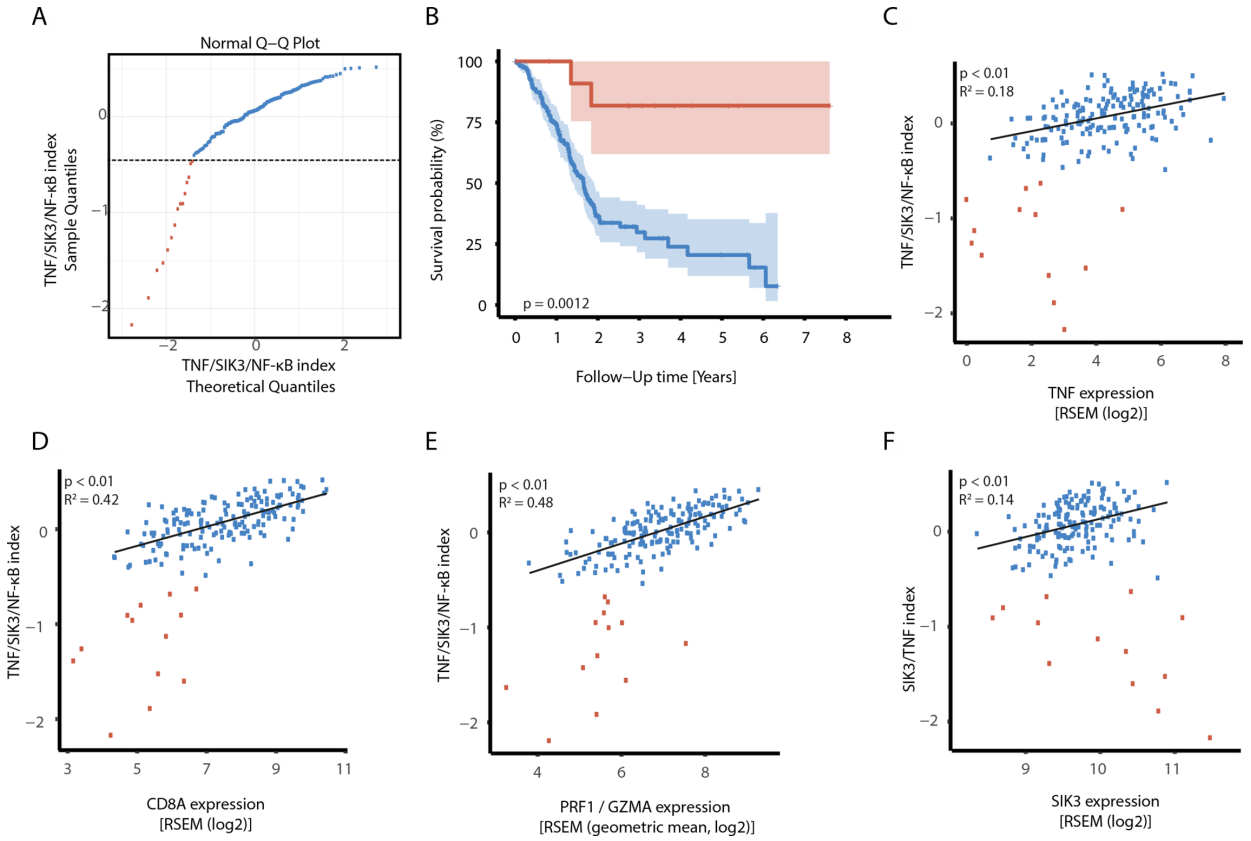

Figure 7 A TNF/SIK3/NF-κB gene signature is associated with poor prognosis in PDAC. (A) Two populations with distinct TNF/SIK3/NF-κB gene signature (index) are observed in patients with PDAC. Q–Q plot of the distribution of the TNF/SIK3 index and a standard Gaussian distribution. The value –0.6 was used as cut-off value to separate index high from index low patients. (B) Patients with low TNF/SIK3/NF-κB index show improved survival than the high TNF/SIK3/NF-κB group. Kaplan-Meier curves with CIs for the index high and low groups. Samples with a low signature index (<–0.6) are shown in red, whereas samples with a high signature index (>0.6) are colored in blue. The estimated p value of 0.0012 indicates a significant better survival in the index low group. (C–F) Expression of selected genes on the x-axis against the TNF/SIK3/NF-κB index signature index on the y-axis. Samples with a signature index of <–0.6 (=low index group) are represented by red circles. In this group, individual samples were numbered for comparison among different graphs. Samples with a signature index of >–0.6 (=high index group) are represented by blue circles. For the high index subgroup, a linear least-squares regression line was fit. We tested whether the slope of this line significantly differs from zero (no correlation) and shows the corresponding p values. (C); TNF correlation coefficient in high index group: 0.423; p value high index <0 .01. (D) CD8A correlation coefficient in the high index group: 0.646; p value of regression <0.01. (E) Geometric mean of perforin (PRF1) and granzyme (GZMA) correlation coefficient in the high index group: 0.695; p value high index <0.01. (F) SIK3 correlation coefficient in the high index group: 0.373; p value high index <0.01. Q–Q, quantile–quantile.

between TC activity in situ and NF-κB activation in the majority of pancreatic cancers. Thus, these data further corroborate the notion that a TNF–SIK3–NF-κB axis promotes tumor progression and that abrogation of this pathway may be beneficial for patients with cancer.

DISCUSSION

The complete success of CIT is hindered by various resistance mechanisms that may originate from the tumor microenvironment or directly from the tumor cells.[2] Recent studies showed that aberrant response to TC-released cytokines is a major mechanism of tumor-intrinsic resistance to immunity.[3 5 6 68] In this work, we show for the first time that tumor cells exploit SIK3 to counteract TC attack by promoting prosurvival gene expression after TNF stimulation. SIK3 was identified by a genetic screen for factors that determine the fate of tumor cells after the encounter of cytotoxic TCs. In contrast to canonical immune modulators, SIK3 critically regulated tumor sensitivity towards TC attack rather than TC activation.

Here, we introduce SIK3 as a molecular switch of TNF responses in cancer. We show that SIK3 sustains TNF-induced NF-κB activation, nuclear translocation, and retention. Along this line, other groups described a modulatory function of SIK family members towards NF-κB activation.[67] Nevertheless, the role of SIK3 in modulating TNF-induced NF-κB activation in the context of cancer immunity has never been reported before. TNF stimulation in SIK3-proficient cancer cells led to profound changes in chromatin accessibility with remarkable alteration of gene expression. Coherently, regulation of chromatin accessibility determines tumor resistance to TC-mediated cytotoxicity.[69 70] In line with other studies,[41 71 72] we showed that NF-κB activation led to massive expression of prosurvival and antiapoptotic genes. Notably, ablation of SIK3 reverted the expression of this gene signature, resulting in massive cell death after TNF stimulation. Overexpression of some of those differentially regulated genes in SIK3-depleted cells conferred only partial protection from TNF-induced cytotoxicity. Based on this observation, we speculate that several SIK3-dependent prosurvival and antiapoptotic genes simultaneously orchestrate protection of tumor cells from TNF or TC-mediated cytotoxicity.

To identify the molecular mechanisms by which SIK3 regulated NF-κB activation, we observed that TNF treatment led to modest but significant activation of the SIK3 upstream kinase LKB1. LKB1 activation from TNF–TNFR1 has never been reported. However, Lombardi *et al* detected higher pLKB1 in macrophages after activation of TLR4 and IL1R,[73] two receptors sharing multiple intracellular signaling nodes with the TNFR1 pathway.[74] Despite the increased LKB1 activation by TNF, knockdown of LKB1 neither increased the sensitivity of tumor cells to TNF nor decreased NF-κB activity. These observations might be explained by the role of LKB1 in modulating the activity of at least 13 different known targets,[75] which overall may have a different impact than the sole inhibition of SIK3. Additionally, LKB1 is a known negative regulator of the NF-κB signaling pathway.[76 77] Hence, we could not confirm a role of LKB1 in activating SIK3 and, in turn, NF-κB on TNF stimulation. Among other reported upstream regulators of SIK3, AKT is activated on TNF stimulation.[78–80] Although we did not address the role of AKT in this work, we hypothesize that SIK3 activation on TNF might occur by this alternative pathway.

To identify the mechanism by which SIK3 influences NF-κB activity, we investigated whether SIK3 modulated known regulators of NF-κB. Strikingly, we observed impaired phosphorylation of IKK and IκBα proteins on SIK3 knockdown. The mechanism by which SIK3 modulates those proteins remains unclear. Yet, SIK3 may promote mTOR activation,[81] which in turn promotes phosphorylation of the IKK complex.[82 83] Alternatively, several NF-κB target genes, such as cFLIP, cIAP2, and XIAP, may generate a feedback loop that in turn sustains the NF-κB pathway by acting on its upstream regulators.[51 84 85] Hence, we propose an indirect role of SIK3 in controlling the upstream regulators of the NF-κB pathway.

On activation, several factors influence the duration and the strength of NF-κB activity.[63] Among them, HDAC4 is a direct target of SIK kinases,[67 86–88] and its phosphorylation by SIK kinases leads to its inactivation.[86] Additionally, HDAC4 physically interacts with p65 subunits of NF-κB and reduces NF-κB stability by deacetylation.[66 67] To link these studies, we showed that knockdown of HDAC4 rescued SIK3-depleted cells from TNF-mediated killing. Thus, we propose a dual role of SIK3 in regulating NF-κB by both promoting IKKα/β and IκBα phosphorylation on the one side and by sustaining NF-κB nuclear retention by inhibiting HDAC4 on the other side.

Despite our validations on the NF-κB transcription factor, chromatin accessibility analysis suggests that additional transcription factors are involved in regulating the observed effects, which we do not rule out. As several of the inferred transcription factors, such as IRF and bZIP family members, are interacting with the NF-κB pathway,[89–91] the observed effects might to some extent be direct effects of NF-κB modulation by SIK3.

To confirm the pivotal role of the TNF–SIK3–NF-κB axis in cancer, we investigated the impact of a TNF–SIK3–NF-κB induced gene signature on patients' survival. The majority of patients with pancreatic cancer showed high gene signature expression, which correlated with poor prognosis. However, patients who were unable to upregulate this gene signature showed prolonged survival. Interestingly enough, SIK3 and TNF expressions did not positively correlate with gene index expression. Whereas we did not further investigate the reasons behind this observation, we speculate that the impaired signature expression may arise from genetic alterations within the TNF–NF-κB pathways that render tumor cells unable to upregulate this signature even in the presence of TNF and SIK3. Taken together, these data confirm that SIK3 protects tumor cells from TC attack by taking advantage

of TC-released TNF to promote profound changes of chromatin accessibility followed by transcription of numerous genes that counteract cytotoxic agents and cytokines released by TCs.

With this work, we sought to provide the rationale of SIK3 as a therapeutic target for CIT. Previously, several studies described roles of SIK3 in promoting cell proliferation, cancer progression, and metastasis.[20 32 33 61 92 93] Hence, SIK3 blockade might decrease tumor proliferation and invasiveness on the one hand and increase tumor susceptibility to TC attack on the other hand. SIK3 expression is not restricted to tumor cells, but SIK3 mRNA is also present in a variety of healthy tissues hinting to possible adverse effects of systemic SIK3 blockade.[94] Yet, abrogation of SIK3 alone did not show a major impact on cell viability, indicating that SIK3 inhibition would induce cytotoxicity only in tissues where TNF is secreted, such as inflamed cancer tissues. Additionally, novel pan-SIK kinase inhibitors did not exert strong toxicity in mice.[95] Such inhibitors have been widely tested in the context of macrophage biology, where they can induce the tolerogenic M2 phenotype.[73] Thereby, SIK2 has been shown to be the driver of this phenotype.[67 73 95–97] Thus, the usage of pan-SIK inhibitors may not be appropriate for cancer treatment, while SIK3-specifc inhibitors might elicit tumor sensitization to immune attack without inducing an immune tolerogenic microenvironment.

Although current cancer therapeutic strategies aim to reinforce TC functionality by acting on immune modulators or cytokine pathways, sensitizing tumor cells to the insult of the immune system may be used as a complementary approach to immunotherapy. In line with these considerations, a recent study showed that lowering TNF cytotoxicity threshold in tumor cells augments the impact of immunotherapy in preclinical models.[5] On the other hand, blockade of TNF failed to show clinical success because of its dual role in cancer.[98] Our work suggests that rewiring tumor response to TNF, by SIK3 inhibition, is a more efficacious strategy to exploit the TNF pathway for anticancer immunity.

Author affiliations
[1]Division of Interventional Immunology, Leibniz Institute for Immunotherapy, Regensburg, Germany
[2]Translational Immunology, German Cancer Research Center (DKFZ), Heidelberg, Germany
[3]Department of Oral and Maxillofacial Surgery, University Hospital Regensburg, Regensburg, Germany
[4]Experimental Medicine and Therapy Research, University of Regensburg, Regensburg, Germany
[5]Signalling and Functional Genomics, German Cancer Research Center (DKFZ), Heidelberg, Germany
[6]Helmholtz-University Group 'Cell Plasticity and Epigenetic Remodeling', German Cancer Research Center (DKFZ), Heidelberg, Germany
[7]Institute of Pathology, University Hospital Heidelberg, Heidelberg, Germany
[8]Institute of Functional Genomics, University of Regensburg, Regensburg, Germany
[9]Molecular Oncology of Gastrointestinal Tumors, German Cancer Research Center (DKFZ), Heidelberg, Germany
[10]DKTK CCU Neuroimmunology and Brain Tumor Immunology, German Cancer Research Center (DKFZ), Heidelberg, Germany
[11]Immune Monitoring Unit, National Center for Tumor Diseases (NCT), Heidelberg, Germany
[12]Joint Immunotherapeutics Laboratory, German Cancer Research Center (DKFZ), Heidelberg, Germany
[13]Research Department, iOmx Therapeutics, Munich/Martinsried, Germany
[14]Department of Internal Medicine III, University Hospital Regensburg, Regensburg, Germany
[15]Functional Genomics, University of Regensburg, Regensburg, Germany
[16]Junior Group 'Epigenetic Immunooncology', Leibniz Institute for Immunotherapy, Regensburg, Germany

Acknowledgements We thank M Lotem for provision of melanoma-derived TIL209 and TIL412; D Männel, Institute of Immunology, University Regensburg, for provision of recombinant tumor necrosis factor; and H Smetak for help with manuscript editing and submission. We also thank the Cooperation Program in Cancer Research of the Deutsches Krebsforschungszentrum and Israel's Ministry of Science, Brigitte Wild, for excellent technical support.

Contributors AS, ANM, TM, VV, FCD, JS, MX, AH, SSt, SSp, NH, JM, KMJ, AR, MWK, DM, OR, CMF, CS, and SP conducted experiments; IP, RO, SP, and ANM generated T cells; AS, NK, TM, MBr, MBo, and PB designed, conducted, and analyzed the genetic screen; CG, MR, AS, CS, and PB analyzed genome or transcriptome data; RS and CK analyzed the patient's data; PB and AS designed the study; AS and PB drafted the manuscript; AS, ANM, FCD, JS, MX, AH, SSt, SSp, NH, JM, MR, CS, and PB revised the manuscript. AS, PB and ANM are the guarantors of this study.

Funding This project was funded by the Deutsche Forschungsgemeinschaft (German Research Foundation) Collaborative Research Program (SFB/TR 221 and Forschergruppe 2127). AH received funding from the European Union's Horizon 2020 research and innovation programme under the Marie Sklodowska-Curie grant agreement No 861190.

Competing interests This work was supported by iOmx Therapeutics AG (Martinsried, Germany).

Patient consent for publication Not applicable.

Ethics approval All in vivo experiments were conducted according to the Federation of European Laboratory Animal Science Associations guidelines.

Provenance and peer review Not commissioned; externally peer reviewed.

Data availability statement Data are available in a public, open access repository. Gene Expression Omnibus public functional genomics data repository (accession code GSE202305).

ORCID iDs
Antonio Sorrentino http://orcid.org/0000-0002-8496-3765
Ayse Nur Menevse http://orcid.org/0000-0002-6024-3464
Franziska Christine Durst http://orcid.org/0000-0001-6714-0321
Maria Xydia http://orcid.org/0000-0001-6057-5330
Abir Hussein http://orcid.org/0000-0002-0063-7867
Philipp Beckhove http://orcid.org/0000-0002-0099-5576

REFERENCES

1 Waldman AD, Fritz JM, Lenardo MJ. A guide to cancer immunotherapy: from T cell basic science to clinical practice. *Nat Rev Immunol* 2020;20:651–68.

2 Sharma P, Hu-Lieskovan S, Wargo JA, *et al*. Primary, adaptive, and acquired resistance to cancer immunotherapy. *Cell* 2017;168:707–23.
3 Kalbasi A, Ribas A. Tumour-Intrinsic resistance to immune checkpoint blockade. *Nat Rev Immunol* 2020;20:25–39.
4 Jenkins RW, Barbie DA, Flaherty KT. Mechanisms of resistance to immune checkpoint inhibitors. *Br J Cancer* 2018;118:9–16.
5 Vredevoogd DW, Kuilman T, Ligtenberg MA, *et al*. Augmenting immunotherapy impact by lowering tumor TNF cytotoxicity threshold. *Cell* 2020;180:404–5.
6 Kearney CJ, Vervoort SJ, Hogg SJ, *et al*. Tumor immune evasion arises through loss of TNF sensitivity. *Sci Immunol* 2018;3:eaar3451.
7 Manguso RT, Pope HW, Zimmer MD, *et al*. In vivo CRISPR screening identifies PTPN2 as a cancer immunotherapy target. *Nature* 2017;547:413–8.
8 Volpin V, Michels T, Sorrentino A, *et al*. CAMK1D triggers immune resistance of human tumor cells refractory to anti-PD-L1 treatment. *Cancer Immunol Res* 2020;8:1163–79.
9 Patel SJ, Sanjana NE, Kishton RJ, *et al*. Identification of essential genes for cancer immunotherapy. *Nature* 2017;548:537–42.
10 Freeman AJ, Kearney CJ, Silke J, *et al*. Unleashing TNF cytotoxicity to enhance cancer immunotherapy. *Trends Immunol* 2021;42:1128–42.
11 Dudley ME, Wunderlich JR, Shelton TE, *et al*. Generation of tumor-infiltrating lymphocyte cultures for use in adoptive transfer therapy for melanoma patients. *J Immunother* 2003;26:332–42.
12 Jin J, Sabatino M, Somerville R, *et al*. Simplified method of the growth of human tumor infiltrating lymphocytes in gas-permeable flasks to numbers needed for patient treatment. *J Immunother* 2012;35:283–92.
13 Khandelwal N, Breinig M, Speck T, *et al*. A high-throughput RNAi screen for detection of immune-checkpoint molecules that mediate tumor resistance to cytotoxic T lymphocytes. *EMBO Mol Med* 2015;7:450–63.
14 Dobin A, Davis CA, Schlesinger F, *et al*. Star: ultrafast universal RNA-seq aligner. *Bioinformatics* 2013;29:15–21.
15 Robinson MD, McCarthy DJ, Smyth GK. edgeR: a Bioconductor package for differential expression analysis of digital gene expression data. *Bioinformatics* 2010;26:139–40.
16 Chen EY, Tan CM, Kou Y, *et al*. Enrichr: interactive and collaborative HTML5 gene list enrichment analysis tool. *BMC Bioinformatics* 2013;14:128.
17 Corces MR, Trevino AE, Hamilton EG, *et al*. An improved ATAC-seq protocol reduces background and enables interrogation of frozen tissues. *Nat Methods* 2017;14:959–62.
18 Wan Y-W, Allen GI, Liu Z. TCGA2STAT: simple TCGA data access for integrated statistical analysis in R. *Bioinformatics* 2016;32:952–4.
19 Beier CP, Kumar P, Meyer K, *et al*. The cancer stem cell subtype determines immune infiltration of glioblastoma. *Stem Cells Dev* 2012;21:2753–61.
20 Schrader A, Meyer K, Walther N, *et al*. Identification of a new gene regulatory circuit involving B cell receptor activated signaling using a combined analysis of experimental, clinical and global gene expression data. *Oncotarget* 2016;7:47061–81.
21 Kassambara A, Kosinski M. *survminer: Drawing Survival Curves using 'ggplot2'. (ed(eds). R package version 0.3.1. edn*, 2017.
22 Anderson AC, Joller N, Kuchroo VK. Lag-3, Tim-3, and TIGIT: Co-inhibitory receptors with specialized functions in immune regulation. *Immunity* 2016;44:989–1004.
23 Ryu K-Y, Maehr R, Gilchrist CA, *et al*. The mouse polyubiquitin gene Ubc is essential for fetal liver development, cell-cycle progression and stress tolerance. *Embo J* 2007;26:2693–706.
24 Liu Q, Guntuku S, Cui X-S, *et al*. Chk1 is an essential kinase that is regulated by Atr and required for the G_2/M DNA damage checkpoint. *Genes Dev* 2000;14:1448–59.
25 MATM vanV, Medema RH. Getting in and out of mitosis with Polo-like kinase-1. 24, 2844-2859 (0000).
26 Coutinho P, Parsons MJ, Thomas KA, *et al*. Differential requirements for COPI transport during vertebrate early development. *Dev Cell* 2004;7:547–58.
27 Sonoda K, Miyamoto S, Nakashima M, *et al*. Receptor-Binding cancer antigen expressed on SiSo cells induces apoptosis via ectodomain shedding. *Exp Cell Res* 2010;316:1795–803.
28 Hsu DK, Chen H-Y, Liu F-T. Galectin-3 regulates T-cell functions. *Immunol Rev* 2009;230:114–27.
29 Liechtenstein T, Dufait I, Bricogne C, *et al*. PD-L1/PD-1 co-stimulation, a brake for T cell activation and a T cell differentiation signal. *J Clin Cell Immunol* 2012;S12:006.
30 Cochaud S, Giustiniani J, Thomas C, *et al*. Il-17A is produced by breast cancer TILs and promotes chemoresistance and proliferation through ERK1/2. *Sci Rep* 2013;3:3456.
31 Hurtado M, Sankpal UT, Kaba A, *et al*. Novel survivin inhibitor for suppressing pancreatic cancer cells growth via downregulating Sp1 and Sp3 transcription factors. *Cell Physiol Biochem* 2018;51:1894–907.
32 Charoenfuprasert S, Yang Y-Y, Lee Y-C, *et al*. Identification of salt-inducible kinase 3 as a novel tumor antigen associated with tumorigenesis of ovarian cancer. *Oncogene* 2011;30:3570–84.
33 Chen H, Huang S, Han X, *et al*. Salt-Inducible kinase 3 is a novel mitotic regulator and a target for enhancing antimitotic therapeutic-mediated cell death. *Cell Death Dis* 2014;5:e1177.
34 Clark K, MacKenzie KF, Petkevicius K, *et al*. Phosphorylation of CRTC3 by the salt-inducible kinases controls the interconversion of classically activated and regulatory macrophages. *Proc Natl Acad Sci U S A* 2012;109:16986–91.
35 Dace DS, Chen PW, Niederkorn JY. Cd8+ T cells circumvent immune privilege in the eye and mediate intraocular tumor rejection by a TNF-alpha-dependent mechanism. *J Immunol* 2007;178:6115–22.
36 Poehlein CH, Hu H-M, Yamada J, *et al*. Tnf plays an essential role in tumor regression after adoptive transfer of perforin/IFN-gamma double knockout effector T cells. *J Immunol* 2003;170:2004–13.
37 Faustman DL, Davis M. Tnf receptor 2 and disease: autoimmunity and regenerative medicine. *Front Immunol* 2013;4:478.
38 MacEwan DJ. TNF ligands and receptors--a matter of life and death. *Br J Pharmacol* 2002;135:855–75.
39 Brenner D, Blaser H, Mak TW. Regulation of tumour necrosis factor signalling: live or let die. *Nat Rev Immunol* 2015;15:362–74.
40 Tang F, Tang G, Xiang J, *et al*. The absence of NF-kappaB-mediated inhibition of c-Jun N-terminal kinase activation contributes to tumor necrosis factor alpha-induced apoptosis. *Mol Cell Biol* 2002;22:8571–9.
41 Beg AA, Baltimore D. An essential role for NF-kappaB in preventing TNF-alpha-induced cell death. *Science* 1996;274:782–4.
42 Karin M, Lin A. Nf-kappaB at the crossroads of life and death. *Nat Immunol* 2002;3:221–7.
43 Baumgart S, Chen N-M, Siveke JT, *et al*. Inflammation-Induced NFATc1-STAT3 transcription complex promotes pancreatic cancer initiation by KrasG12D. *Cancer Discov* 2014;4:688–701.
44 Buchholz M, Schatz A, Wagner M, *et al*. Overexpression of c-myc in pancreatic cancer caused by ectopic activation of NFATc1 and the Ca2+/calcineurin signaling pathway. *Embo J* 2006;25:3714–24.
45 Oikawa T, Nakamura A, Onishi N, *et al*. Acquired expression of NFATc1 downregulates E-cadherin and promotes cancer cell invasion. *Cancer Res* 2013;73:5100–9.
46 Singh SK, Chen N-M, Hessmann E, *et al*. Antithetical NFATc1-Sox2 and p53-miR200 signaling networks govern pancreatic cancer cell plasticity. *Embo J* 2015;34:517–30.
47 Baldwin AS. Control of oncogenesis and cancer therapy resistance by the transcription factor NF-kappaB. *J Clin Invest* 2001;107:241–6.
48 Tamura K, Makino A, Hullin-Matsuda F, *et al*. Novel lipogenic enzyme ELOVL7 is involved in prostate cancer growth through saturated long-chain fatty acid metabolism. *Cancer Res* 2009;69:8133–40.
49 Priem D, Devos M, Druwé S, *et al*. A20 protects cells from TNF-induced apoptosis through linear ubiquitin-dependent and -independent mechanisms. *Cell Death Dis* 2019;10:692.
50 Tewari M, Wolf FW, Seldin MF, *et al*. Lymphoid expression and regulation of A20, an inhibitor of programmed cell death. *J Immunol* 1995;154:1699–706.
51 Mahoney DJ, Cheung HH, Mrad RL, *et al*. Both cIAP1 and cIAP2 regulate TNFalpha-mediated NF-kappaB activation. *Proc Natl Acad Sci U S A* 2008;105:11778–83.
52 Yu H, Lin L, Zhang Z, *et al*. Targeting NF-κB pathway for the therapy of diseases: mechanism and clinical study. *Signal Transduct Target Ther* 2020;5:209.
53 Micheau O, Lens S, Gaide O, *et al*. Nf-kappaB signals induce the expression of c-FLIP. *Mol Cell Biol* 2001;21:5299–305.
54 Liu H, Yang J, Yuan Y, *et al*. Regulation of Mcl-1 by constitutive activation of NF-κB contributes to cell viability in human esophageal squamous cell carcinoma cells. *BMC Cancer* 2014;14:98.
55 Joung J, Kirchgatterer PC, Singh A, *et al*. Crispr activation screen identifies Bcl-2 proteins and B3GNT2 as drivers of cancer resistance to T cell-mediated cytotoxicity. *Nat Commun* 2022;13:1606.
56 Lin Y, Bai L, Chen W, *et al*. The NF-kappaB activation pathways, emerging molecular targets for cancer prevention and therapy. *Expert Opin Ther Targets* 2010;14:45–55.
57 Wertz IE, O'Rourke KM, Zhou H, *et al*. De-Ubiquitination and ubiquitin ligase domains of A20 downregulate NF-kappaB signalling. *Nature* 2004;430:694–9.
58 Boone DL, Turer EE, Lee EG, *et al*. The ubiquitin-modifying enzyme A20 is required for termination of Toll-like receptor responses. *Nat Immunol* 2004;5:1052–60.

59 Düwel M, Welteke V, Oeckinghaus A, *et al*. A20 negatively regulates T cell receptor signaling to NF-kappaB by cleaving MALT1 ubiquitin chains. *J Immunol* 2009;182:7718–28.
60 Verstrepen L, Verhelst K, van Loo G, *et al*. Expression, biological activities and mechanisms of action of A20 (TNFAIP3). *Biochem Pharmacol* 2010;80:2009–20.
61 Sun Z, Jiang Q, Li J, *et al*. The potent roles of salt-inducible kinases (SIKs) in metabolic homeostasis and tumorigenesis. *Signal Transduct Target Ther* 2020;5:150.
62 Walkinshaw DR, Weist R, Kim G-W, *et al*. The tumor suppressor kinase LKB1 activates the downstream kinases SIK2 and SIK3 to stimulate nuclear export of class IIa histone deacetylases. *J Biol Chem* 2013;288:9345–62.
63 Ghosh S, Hayden MS. New regulators of NF-kappaB in inflammation. *Nat Rev Immunol* 2008;8:837–48.
64 Webster JD, Vucic D. The balance of TNF mediated pathways regulates inflammatory cell death signaling in healthy and diseased tissues. *Front Cell Dev Biol* 2020;8:365.
65 Rothgiesser KM, Fey M, Hottiger MO. Acetylation of p65 at lysine 314 is important for late NF-kappaB-dependent gene expression. *BMC Genomics* 2010;11:22.
66 Chen L-feng, Mu Y, Greene WC. Acetylation of RelA at discrete sites regulates distinct nuclear functions of NF-kappaB. *Embo J* 2002;21:6539–48.
67 Luan B, Goodarzi MO, Phillips NG, *et al*. Leptin-Mediated increases in catecholamine signaling reduce adipose tissue inflammation via activation of macrophage HDAC4. *Cell Metab* 2014;19:1058–65.
68 Shen Y, Eng JS, Fajardo F, *et al*. Cancer cell-intrinsic resistance to bite therapy is mediated by loss of CD58 costimulation and modulation of the extrinsic apoptotic pathway. *J Immunother Cancer* 2022;10:e004348.
69 Pan D, Kobayashi A, Jiang P, *et al*. A major chromatin regulator determines resistance of tumor cells to T cell-mediated killing. *Science* 2018;359:770–5.
70 Wellinger LC, Hogg SJ, Newman DM, *et al*. Bet inhibition enhances TNF-mediated antitumor immunity. *Cancer Immunol Res* 2022;10:87–107.
71 Rivas MA, Carnevale RP, Proietti CJ, *et al*. Tnf alpha acting on TNFR1 promotes breast cancer growth via p42/p44 MAPK, JNK, Akt and NF-kappa B-dependent pathways. *Exp Cell Res* 2008;314:509–29.
72 Hoesel B, Schmid JA. The complexity of NF-κB signaling in inflammation and cancer. *Mol Cancer* 2013;12:86.
73 Lombardi MS, Gilliéron C, Dietrich D, *et al*. Sik inhibition in human myeloid cells modulates TLR and IL-1R signaling and induces an anti-inflammatory phenotype. *J Leukoc Biol* 2016;99:711–21.
74 Verstrepen L, Bekaert T, Chau T-L, *et al*. Tlr-4, IL-1R and TNF-R signaling to NF-kappaB: variations on a common theme. *Cell Mol Life Sci* 2008;65:2964–78.
75 Lizcano JM, Göransson O, Toth R, *et al*. Lkb1 is a master kinase that activates 13 kinases of the AMPK subfamily, including MARK/PAR-1. *Embo J* 2004;23:833–43.
76 Buensuceso A, Fritz JL, Collins O, *et al*. Loss of LKB1-NUAK1 signalling enhances NF-κB activity in a spheroid model of high-grade serous ovarian cancer. *Sci Rep* 2022;12:3011.
77 Yuan Y, Li S-L, Cao Y-L, *et al*. Lkb1 suppresses glioma cell invasion via NF-κB/Snail signaling repression. *Onco Targets Ther* 2019;12:2451–63.
78 Faurschou A, Gniadecki R. Tnf-Alpha stimulates Akt by a distinct aPKC-dependent pathway in premalignant keratinocytes. *Exp Dermatol* 2008;17:992–7.
79 Zhou Z, Gengaro P, Wang W, *et al*. Role of NF-kappaB and Pi 3-kinase/Akt in TNF-alpha-induced cytotoxicity in microvascular endothelial cells. *Am J Physiol Renal Physiol* 2008;295:F932–41.
80 Choi S, Lim D-S, Chung J. Feeding and fasting signals converge on the LKB1-SIK3 pathway to regulate lipid metabolism in Drosophila. *PLoS Genet* 2015;11:e1005263.
81 Ponnusamy L, Kothandan G, Manoharan R. Berberine and emodin abrogates breast cancer growth and facilitates apoptosis through inactivation of SIK3-induced mTOR and Akt signaling pathway. *Biochim Biophys Acta Mol Basis Dis* 2020;1866:165897.
82 Dan HC, Cooper MJ, Cogswell PC, *et al*. Akt-dependent regulation of NF-{kappa}B is controlled by mTOR and Raptor in association with IKK. *Genes Dev* 2008;22:1490–500.
83 Ahmad A, Biersack B, Li Y, *et al*. Targeted regulation of PI3K/Akt/mTOR/NF-κB signaling by indole compounds and their derivatives: mechanistic details and biological implications for cancer therapy. *Anticancer Agents Med Chem* 2013;13:1002–13.
84 Hofer-Warbinek R, Schmid JA, Stehlik C, *et al*. Activation of NF-kappa B by XIAP, the X chromosome-linked inhibitor of apoptosis, in endothelial cells involves TAK1. *J Biol Chem* 2000;275:22064–8.
85 Fiore A, Ugel S, De Sanctis F, *et al*. Induction of immunosuppressive functions and NF-κB by FLIP in monocytes. *Nat Commun* 2018;9:5193.
86 Henriksson E, Säll J, Gormand A, *et al*. Sik2 regulates CRTCs, HDAC4 and glucose uptake in adipocytes. *J Cell Sci* 2015;128:472–86.
87 Patel K, Foretz M, Marion A, *et al*. The LKB1-salt-inducible kinase pathway functions as a key gluconeogenic suppressor in the liver. *Nat Commun* 2014;5:4535.
88 Darling NJ, Cohen P. Nuts and bolts of the salt-inducible kinases (SIKs). *Biochem J* 2021;478:1377–97.
89 Platanitis E, Decker T. Regulatory networks involving STATs, IRFs, and NFκB in inflammation. *Front Immunol* 2018;9:2542.
90 Iwanaszko M, Kimmel M. NF-κB and IRF pathways: cross-regulation on target genes promoter level. *BMC Genomics* 2015;16:307.
91 de Oliveira KAP, Kaergel E, Heinig M, *et al*. A roadmap of constitutive NF-κB activity in Hodgkin lymphoma: dominant roles of p50 and p52 revealed by genome-wide analyses. *Genome Med* 2016;8:28.
92 Amin N, Khan A, St Johnston D, *et al*. Lkb1 regulates polarity remodeling and adherens junction formation in the Drosophila eye. *Proc Natl Acad Sci U S A* 2009;106:8941–6.
93 Wehr MC, Holder MV, Gailite I, *et al*. Salt-Inducible kinases regulate growth through the Hippo signalling pathway in Drosophila. *Nat Cell Biol* 2013;15:61–71.
94 Uebi T, Itoh Y, Hatano O, *et al*. Involvement of SIK3 in glucose and lipid homeostasis in mice. *PLoS One* 2012;7:e37803.
95 Sundberg TB, Liang Y, Wu H, *et al*. Development of chemical probes for investigation of salt-inducible kinase function in vivo. *ACS Chem Biol* 2016;11:2105–11.
96 MacKenzie KF, Clark K, Naqvi S, *et al*. PGE $_2$Induces Macrophage IL-10 Production and a Regulatory-like Phenotype via a Protein Kinase A–SIK–CRTC3 Pathway. *J.i.* 2013;190:565–77.
97 Darling NJ, Toth R, Arthur JSC, *et al*. Inhibition of SIK2 and SIK3 during differentiation enhances the anti-inflammatory phenotype of macrophages. *Biochem J* 2017;474:521–37.
98 Montfort A, Colacios C, Levade T, *et al*. The TNF paradox in cancer progression and immunotherapy. *Front Immunol* 2019;10:1818.

Supplementary Information

Salt-inducible kinase 3 protects tumor cells from cytotoxic T cell attack by promoting TNF-induced NF-κB activation

Antonio Sorrentino, Ayse Nur Menevse, Tillmann Michels, Valentina Volpin, Franziska Christine Durst, Julian Sax, Maria Xydia, Abir Hussein, Slava Stamova, Steffen Spörl, Nicole Heuschneider, Jasmin Mühlbauer, Katharina Marlene Jeltsch, Anchana Rathinasamy, Melanie Werner-Klein, Marco Breinig, Damian Mikietyn, Christian Kohler, Isabel Poschke, Sabrina Purr, Olivia Reidell, Catarina Martins Freire, Rienk Offringa, Claudia Gebhard, Rainer Spang, Michael Rehli, Michael Boutros, Christian Schmidl, Nisit Khandelwal, Philipp Beckhove

Supplementary Figures

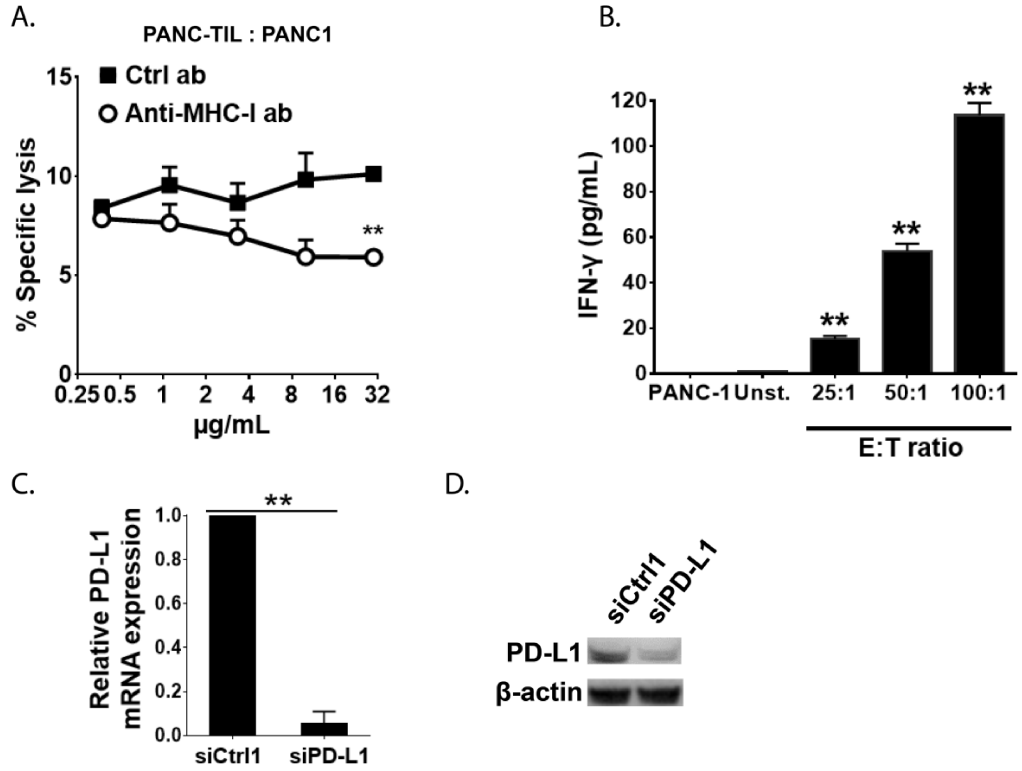

Figure S1. Setup of a HT-screening for novel immune modulators in pancreatic cancer.

(A) Chromium release assay for detection of T cell mediated cytotoxicity in the presence of the indicated concentrations of anti-MHC-I antibody (white symbols) or IgG2a isotype control (black symbols). PANC-TIL and PANC-1 cells were co-cultured for 6h at E:T ratio = 50:1. **(B)** TIL#1 and PANC-1 cells were co-cultured for 24h at the indicated E:T ratios. IFN-γ secretion was measured by ELISA: As negative control, T cells were cultured in the absence of tumor cells (Unst.). **(C)** Quantitative PCR (qPCR) analysis of PD-L1 mRNA expression in PANC-1 cells after siRNA transfection. Results are presented in terms of fold change after normalizing to β-actin. **(D)** Western blot analysis for the detection of PD-L1 protein in PANC-1 cells 72h after siRNA transfection. Graph shows representative data of at least two independent experiments. Graph shows mean +/- SEM. P-values were calculated using two-tailed student´s t-test. * $p < 0.05$, **$p<0.01$.

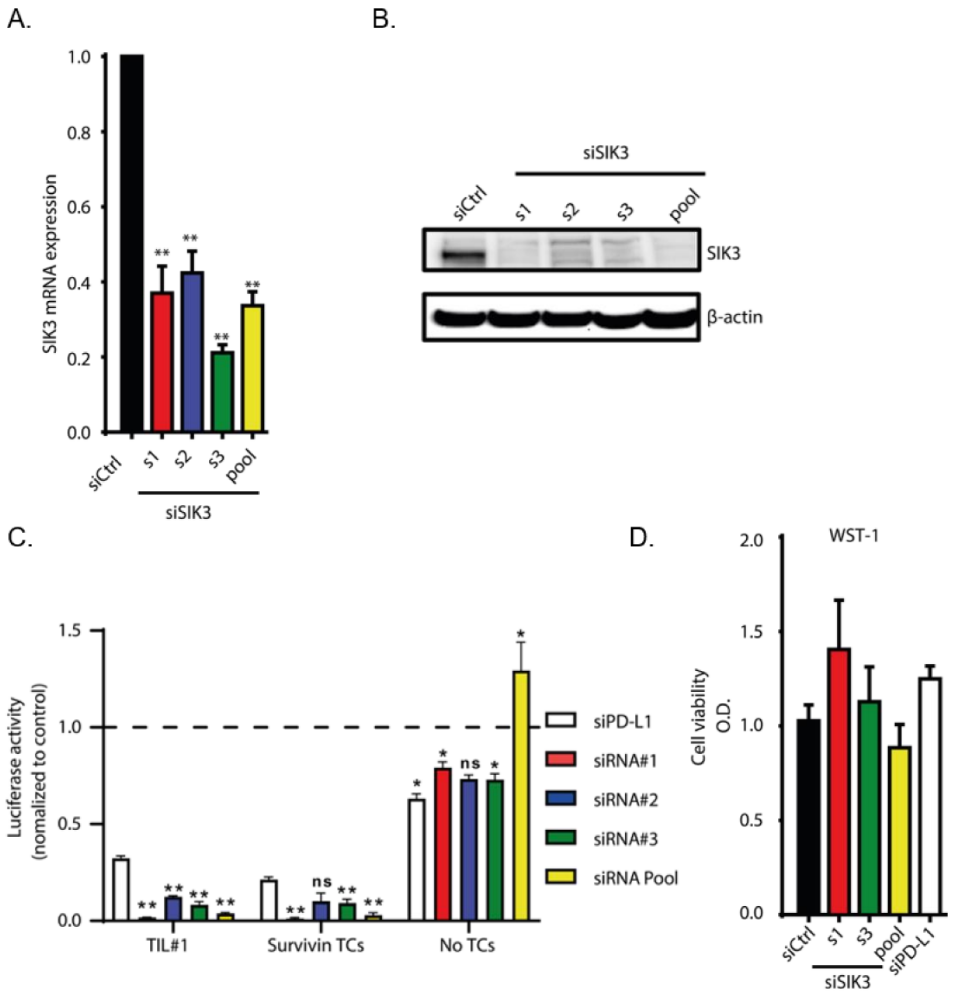

Figure S2. Assessment of SIK3-specific siRNAs' efficiency and cell viability.

(A) PANC-1-luc cells were transfected either with single (s#) or pooled (pool) siRNA sequences targeting SIK3. Scramble siRNA was used as control (siCtrl). After 72h, mRNA expression was evaluated using qPCR. Data were normalized to GAPDH. **(B)** Western blot analysis for knockdown efficiency of SIK3 using SIK3-targeting siRNAs. siRNA transfection in PANC-1-luc cells was performed as in (A). **(C)** Relative to Figure 2A. SIK3 knockdown induces stronger T cell mediated killing than PD-L1 knockdown. Unpaired t-test was conducted comparing each individual siRNA targeting SIK3 against PD-L1 knockdown, for each treatment. **(D)** Effect of SIK3-specific siRNA sequences on tumor cell viability assessed by WST-1 assay. PANC-1 cells were transfected with indicated siRNAs for 72h. Data were normalized to siCtrl. (A and C) Cumulative data of three independent experiments. Bars show mean +/- SEM values. p-values were calculated using two-tailed student´s t-test. * $p < 0.05$, ** $p < 0.01$.

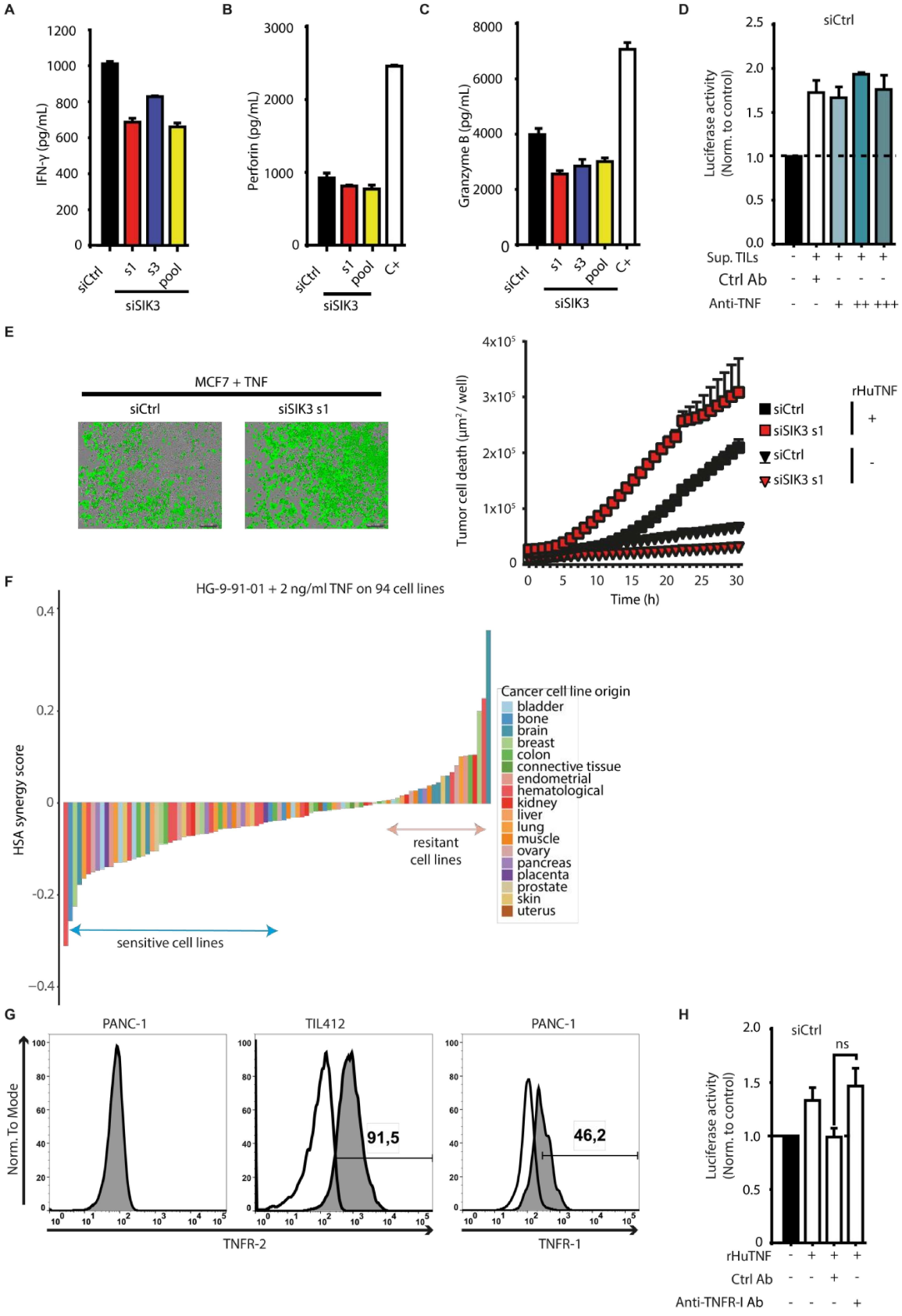
A
IFN-γ (pg/mL)
siCtrl
s1
s3
pool
siSIK3
B
Perforin (pg/mL)
C+
C
Granzyme B (pg/mL)
D
siCtrl
Luciferase activity (Norm. to control)
Sup. TILs
Ctrl Ab
Anti-TNF
E
MCF7 + TNF
siSIK3 s1
Tumor cell death (µm² / well)
Time (h)
rHuTNF
F
HG-9-91-01 + 2 ng/ml TNF on 94 cell lines
HSA synergy score
resitant cell lines
sensitive cell lines
Cancer cell line origin
bladder
bone
brain
breast
colon
connective tissue
endometrial
hematological
kidney
liver
lung
muscle
ovary
pancreas
placenta
prostate
skin
uterus
G
PANC-1
TIL412
Norm. To Mode
91,5
46,2
TNFR-2
TNFR-1
H
ns
rHuTNF
Ctrl Ab
Anti-TNFR-I Ab

Figure S3. SIK3 regulates tumor cell sensitivity to TNF.

(A) IFN-γ ELISA. PANC-1 cells were transfected with the indicated SIK3-specific siRNAs (s1, s3, pool) or scrambled siRNA (siCtrl) for 72h. Afterwards, survivin-specific TCs were added (E:T = 5:1) and after 20h INF- γ secretion was measured in co-culture supernatants. Representative data of two independent experiments. **(B)** Perforin ELISA. M579 cells were transfected as in (A) and co-cultured with TIL209 (E:T = 5:1). Perforin secretion was determined in supernatants 20h after co-culture. Phorbol 12-myristate 13-acetate (PMA)/Ionomycin stimulation served as positive control (C+). Representative data of two independent experiments. **(C)** Granzyme B ELISA. PANC-1 cells were transfected as in (A) and PANC-TIL were added at E:T = 50:1. Granzyme B secretion was measured after 20h in co-culture supernatants. Representative data of two independent experiments. **(D)** Supernatant from CD3/CD28 bead-stimulated T cells was pre-incubated with 100 (+), 300 (++) or 900 (+++) ng/ml of anti-TNF neutralizing antibody for 30 min. Isotype control (Ctrl Ab) was used at concentration of 900 ng/ml. siCtrl transfected PANC-1-luc cells were subjected to the pre-treated supernatant or control medium for 24h and cytotoxicity was measured using luciferase-based killing assay. Data are presented as fold change to unstimulated control. Cumulative data of 3 independent experiments are shown. **(E).** Effect of 100 ng/ml rHuTNF treatment on the viability of MCF-7 cells that were transfected either with siCtrl or with siSIK3 s1. The graph indicates apoptotic tumor cells as determined by the area of YOYO-1+ cells (μm^2/well). **(F)** A panel of 94 human cell lines was plated for 48 h before addition of 2 ng/ml rHuTNF and 6 different concentrations of HG-9-91-01 (1 µM- 1 nM) and incubated for 120 h. Afterwards, the optical density was analyzed using the SRB method as a measure of growth. Dose-response curves were fitted to the data (non-linear regression) and the highest single agent (HSA) model was used to calculate synergy effects. Synergy and resistance to the combination of rHu TNF and HG-9-91-01 are shown in the waterfall plot. Representative data of two independent experiments. **(G)** TNFR-2 (left panel) and TNFR-1 (right panel) expression on PANC-1 cells. TIL412 were used as positive control for TNFR-2 expression. Histograms show live, single cells after staining with primary anti-TNFR-1 or anti-TNFR-2 antibodies and PE-labelled secondary antibody. White histogram: isotype control, grey histogram: anti-TNFR-1 or anti-TNFR-2 as indicated. **(H)** Effect of TNFR-1 blockade on siCtrl transfected PANC-1-luc cells after treatment with 100 ng/mL of rHuTNF as determined by luciferase intensity. Cumulative data of three independent experiments. (A-C, F) Representative data of two independent experiments. (A-D, H) Columns show mean +/- SEM. P-values were calculated using two-tailed student´s t-test. * $p < 0.05$, ** $p < 0.01$.

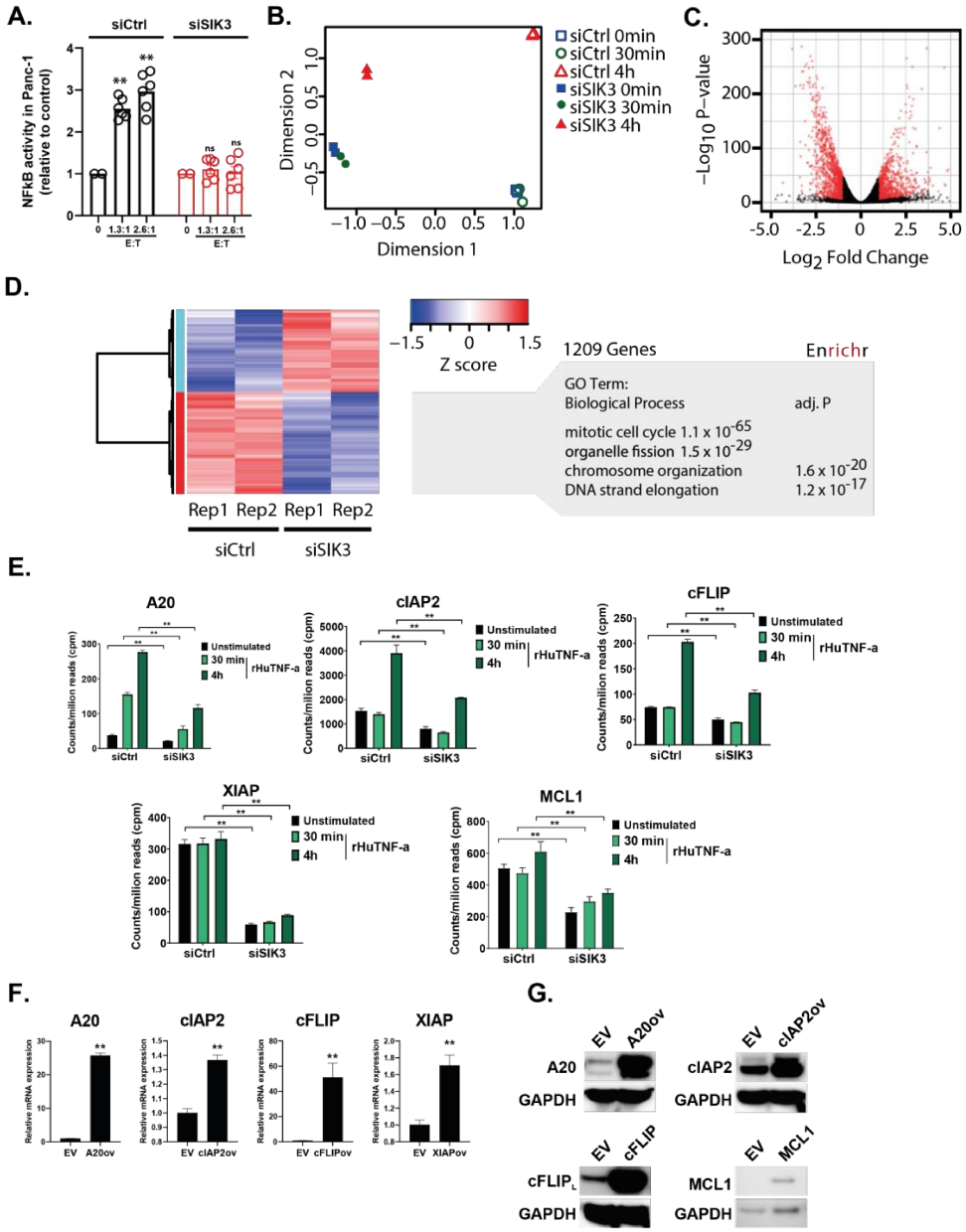

Figure S4. Effect of SIK3 knockdown on tumor cell transcription.

(A) NF-κB reporter assay**.** PANC-1 cells, carrying the luciferase gene under the control of NF-κB promoter, were transfected with the indicated siRNAs for 72h**.** Afterwards, tumor cells were co-cultured with FluT cells at the indicated E:T ratio for 12h. Tumor cells were lysed and luciferase activity was measured**. (B)** PANC-1 cells were treated with siCtrl or siSIK3 for 72h. Afterwards, TNF stimulation was applied for 30min and 4h and gene expression levels were measured using RNAseq. The multidimensional scaling (MDS) plot for replicate RNAseq data sets shows that siRNA and TNF treatment separate samples by at least 1 dimension. **(C)** Volcano Plot highlighting differentially expressed genes after SIK3 knockdown alone (fold change ≥ 2, normalized counts per million > 2, FDR ≤ .05). Red dots = genes with significant differential expression. **(D)** Two-dimensional hierarchical clustering of 2185 differentially

expressed genes (Z-score transformed, normalized counts per million; Manhattan distance, Ward method). The right panel shows representative gene enrichment analysis results for genes downregulated after SIK3 knockdown. **(E)** Related to Figure 5A: Results from the RNAseq experiment were plotted for individual genes of interest. **(F)** qPCR for the detection of overexpression level in PANC 1 cells transfected with ORF for NF-κB target genes. Data were normalized to GAPDH. **(G)** Representative WB for the assessment of protein expression in PANC-1 cells upon stable transfection with ORF for NF-κB target genes. GAPDH was used as loading control. **(F-G)** Representative data of at least two independent experiments. Columns show mean +/- SEM P-values were calculated using two-tailed student´s t-test. * $p < 0.05$, ** $p < 0.01$.

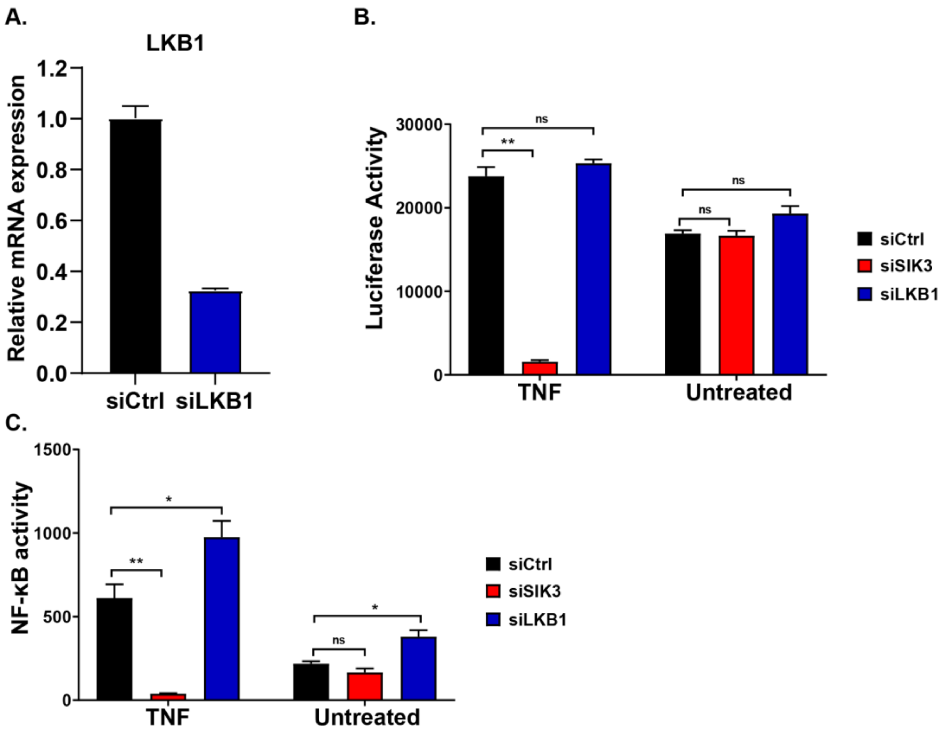

Figure S5. Role of LKB1 in regulating SIK3-mediated effects.

(A) qPCR for the detection of LKB1 mRNA levels in PANC-1 cells upon transfection of LKB1-specific siRNA. **(B)** Luciferase-based cytotoxicity assay. PANC-1 cells were transfected with the indicated siRNA, afterwards TNF stimulation (100ng/mL) was applied for 24h. Luciferase readout was performed as described in materials and methods. **(C)** NF-κB reported assay. PANC-1 cells, carrying the luciferase gene under the control of NF-κB promoter, were transfected with the indicated siRNAs for 72h**.** Afterwards, cells were stimulated with 100ng/mL of rHuTNF for 24h. Tumor cells were lysed and luciferase activity was measured. Representative data of at least two independent experiments. Columns show mean +/- SEM P-values were calculated using two-tailed student´s t-test. * $p < 0.05$, ** $p < 0.01$

Supplementary Tables

Table S2

Cell line	Normalized		Raw		Normalized		Synergy
	IC50 no TNF	IC50 + TNF	IC50 no TNF	IC50 + TNF	GI50 no TNF	GI50 + TNF	**Average HSA**
22RV1	No IC50	No IC50	No IC50	No IC50	No GI50	No GI50	-0,0080
5637	No IC50	No IC50	No IC50	No IC50	No GI50	No GI50	-0,0304
7860	8,67E-07	1,28E-06	7,78E-07	1,01E-06	8,67E-07	1,14E-06	-0,0267
A204	2,09E-07	TNF-induced apoptosis	2,18E-07	TNF-induced apoptosis	2,09E-07	No GI50	0,0365
A2780	No IC50	No IC50	No IC50	No IC50	No GI50	No GI50	0,0248
A375	No IC50	No IC50	No IC50	No IC50	No GI50	No GI50	-0,1146
A431	No IC50	No IC50	No IC50	No IC50	No GI50	No GI50	0,0575
A549	No IC50	No IC50*	No IC50	7,55E-07	No GI50	No GI50	-0,0540
A673	No IC50	No IC50	No IC50	No IC50	No GI50	No GI50	0,0253
ACHN	2,92E-07	8,74E-07	2,97E-07	2,87E-07	2,92E-07	5,75E-07	-0,0701
ASPC1	2,55E-05	No IC50	4,80E-05	No IC50	2,55E-05	No GI50	-0,0653
BT20	No IC50	TNF-induced apoptosis	No IC50	TNF-induced apoptosis	No GI50	No GI50	0,0000
BXPC3	No IC50	No IC50	No IC50	No IC50	No GI50	No GI50	-0,0499
C33A	5,87E-07	2,61E-06	1,22E-06	2,37E-05	5,87E-07	8,53E-07	-0,0125
CACO2	No IC50	No IC50	No IC50	No IC50	No GI50	No GI50	-0,0557
CAKI1	5,17E-08	6,40E-08	5,24E-08	1,29E-07	5,17E-08	1,02E-07	0,1038
CALU6	No IC50	TNF-induced apoptosis	No IC50	TNF-induced apoptosis	No GI50	No GI50	-0,1286
CASKI	No IC50	No IC50	No IC50	No IC50	No GI50	No GI50	-0,1375
CLS439	1,05E-06	5,66E-07	8,97E-07	5,71E-07	1,05E-06	4,86E-07	0,0060
COLO205	No IC50	TNF-induced apoptosis	5,12E-05	TNF-induced apoptosis	No GI50	No GI50	-0,0165
COLO678	No IC50	No IC50	No IC50	No IC50	No GI50	No GI50	-0,0080

DLD1	No IC50	No IC50	No IC50	No IC50	No GI50	No GI50	-0,0377
DU145	No IC50	No IC50	No IC50	No IC50	No GI50	No GI50	-0,1037
EFO21	No IC50	No IC50	No IC50	No IC50	No GI50	No GI50	-0,0376
EJ28	1,23E-06	7,15E-06	1,22E-06	4,72E-06	1,23E-06	2,83E-06	-0,0104
GRANTA-519	No IC50	No IC50	No IC50	1,36E-04	No GI50	No GI50	-0,0632
HCT116	No IC50	No IC50	No IC50	8,52E-07	No GI50	No GI50	-0,1168
HCT15	No IC50	No IC50	No IC50	No IC50	No GI50	No GI50	-0,0879
HEK2913	No IC50	No IC50	No IC50	No IC50	No GI50	No GI50	0,0172
HELA	2,62E-06	No IC50	2,95E-06	No IC50	2,62E-06	No GI50	0,1014
HEPG2	No IC50	No IC50	No IC50	No IC50	No GI50	No GI50	-0,1041
HL-60	No IC50	2,52E-07	1,19E-06	1,31E-07	No GI50	2,62E-07	-0,3095
HS578T	2,51E-07	6,83E-07	2,34E-07	6,15E-07	2,51E-07	3,03E-07	0,0039
HS729	No IC50	No IC50	No IC50	No IC50	No GI50	No GI50	-0,0529
HT1080	No IC50	No IC50	No IC50	No IC50	No GI50	No GI50	-0,0099
HT29	No IC50	No IC50	No IC50	No IC50	No GI50	No GI50	-0,0146
IGROV1	3,71E-07	4,97E-07	3,60E-07	5,37E-07	3,71E-07	4,90E-07	0,0802
IMR90	3,73E-08	1,62E-07	1,03E-07	3,66E-07	3,73E-08	2,06E-07	0,0998
J82	No IC50	1,11E-06	No IC50	7,32E-07	No GI50	9,61E-07	-0,1284
JAR	No IC50	4,73E-07	No IC50	3,29E-07	No GI50	4,49E-07	-0,0407
JEG3	No IC50	No IC50	No IC50	No IC50	No GI50	No GI50	-0,1376
JIMT1	No IC50	No IC50	No IC50	No IC50	No GI50	No GI50	-0,0202
K-562	2,60E-07	2,68E-07	2,58E-07	1,92E-07	2,60E-07	2,60E-07	-0,0487
KASUMI-1	No IC50	TNF-induced apoptosis	5,41E-08	TNF-induced apoptosis	5,67E-08	5,67E-08	-0,0443
L-363	2,49E-07	2,62E-07	2,41E-07	2,43E-07	2,49E-07	2,49E-07	-0,0847
LOVO	No IC50	3,87E-07	No IC50	8,61E-07	No GI50	5,29E-07	0,1035
MCF7	No IC50	No IC50	No IC50	No IC50	No GI50	2,78E-05	0,0099

MDAMB231	No IC50	No IC50	3,10E-07	2,80E-06	No GI50	7,20E-06	-0,0884
MDAMB435	No IC50	No IC50	No IC50	1,02E-07	No GI50	No GI50	-0,0728
MDAMB436	No IC50	No IC50	No IC50	No IC50	No GI50	No GI50	-0,0657
MDAMB468	No IC50	No IC50	1,00E-09	No IC50	No GI50	No GI50	-0,2239
MG63	No IC50	No IC50	No IC50	No IC50	No GI50	No GI50	-0,0393
MHHES1	1,33E-05	No IC50	1,71E-05	No IC50	1,33E-05	No GI50	-0,0155
MIAPACA2	7,76E-07	4,21E-07	7,89E-07	1,22E-07	7,76E-07	3,36E-07	-0,0537
MINO	3,93E-07	3,93E-07	3,89E-07	3,04E-07	3,93E-07	3,33E-07	-0,1240
MT3	No IC50	No IC50	MT3	No IC50	No GI50	No GI50	-0,0102
MV4-11	No IC50	TNF-induced apoptosis	5,96E-08	TNF-induced apoptosis	6,57E-08	No GI50	-0,0802
NCIH292	6,64E-07	No IC50	6,66E-07	No IC50	6,64E-07	No GI50	-0,0609
NCIH358M	No IC50	No IC50	No IC50	No IC50	No GI50	No GI50	-0,1628
NCIH460	No IC50	No IC50	No IC50	No IC50	No GI50	No GI50	-0,0301
NCIH82	No IC50	No IC50	No IC50	No IC50	No GI50	No GI50	-0,0130
OVCAR3	4,18E-07	3,86E-07	4,03E-07	1,49E-07	4,18E-07	2,20E-07	-0,1490
OVCAR4	3,00E-06	No IC50	3,80E-06	No IC50	3,00E-06	No GI50	-0,0792
PANC1	3,52E-06	7,13E-07	4,34E-06	3,80E-08	3,52E-06	5,24E-07	-0,1456
PANC1005	No IC50	No IC50	No IC50	No IC50	No GI50	No GI50	0,0305
PBMC	No IC50	No IC50	No IC50	No IC50	No GI50	No GI50	0,2263
PC3	6,84E-07	2,20E-06	7,29E-07	1,13E-06	6,84E-07	1,18E-06	-0,0673
PLCPRF5	No IC50	No IC50	No IC50	No IC50	No GI50	No GI50	0,0148
RAMOS	No IC50	No IC50	No IC50	No IC50	No GI50	No GI50	0,0659
RD	1,16E-06	1,33E-06	1,29E-06	1,25E-06	1,16E-06	9,60E-07	-0,0329
RDES	No IC50	No IC50	No IC50	No IC50	No GI50	No GI50	0,0300
SAOS2	5,51E-07	No IC50	3,68E-07	2,52E-07	5,51E-07	1,89E-07	-0,2555
SF268	1,38E-06	No IC50	1,52E-06	No IC50	1,38E-06	No GI50	0,0385
SF295	3,60E-04	No IC50	8,65E-05	1,88E-07	3,60E-04	No GI50	-0,1101

SKBR3	No IC50	No IC50	No IC50	No IC50	No GI50	No GI50	0,1990
SKHEP1	No IC50	No IC50	No IC50	No IC50	No GI50	No GI50	-0,0499
SKLMS1	No IC50	No IC50	No IC50	No IC50	No GI50	No GI50	-0,0160
SKMEL28	No IC50	No IC50	No IC50	No IC50	No GI50	No GI50	-0,0489
SKMEL5	No IC50	No IC50	No IC50	No IC50	No GI50	No GI50	-0,1276
SKNAS	2,43E-07	No IC50	2,20E-07	5,40E-08	2,43E-07	No GI50	-0,1765
SKNSH	No IC50	No IC50	No IC50	No IC50	No GI50	No GI50	0,0582
SKOV3	7,54E-07	No IC50	6,60E-07	6,45E-07	7,54E-07	7,54E-07	-0,0523
SNB75	4,03E-07	No IC50	3,36E-07	No IC50	4,03E-07	No GI50	0,0430
SU-DHL-10	No IC50	No IC50	No IC50	No IC50	No GI50	No GI50	-0,0295
SU-DHL-6	2,81E-07	No IC50	2,56E-07	4,09E-07	2,81E-07	4,50E-07	-0,0705
SW620	No IC50	No IC50	No IC50	No IC50	No GI50	No GI50	0,0020
T24	7,58E-07	5,05E-07	7,69E-07	6,56E-08	7,58E-07	7,58E-07	-0,1429
TE671	No IC50	No IC50	No IC50	No IC50	No GI50	No GI50	0,0050
THP-1	9,26E-08	8,97E-08	8,70E-08	2,84E-08	9,26E-08	7,52E-08	-0,1536
U2OS	7,91E-07	3,75E-07	7,98E-07	4,31E-07	7,91E-07	7,91E-07	-0,0364
U87MG	No IC50	No IC50	1,21E-105	No IC50	No GI50	No GI50	0,3508
UMUC3	4,73E-07	5,41E-07	4,58E-07	1,83E-07	4,73E-07	4,52E-07	-0,1205
UO31	1,82E-07	5,50E-07	1,76E-07	1,76E-07	1,82E-07	1,82E-07	-0,0037
WSU-NHL	2,67E-07	3,73E-07	2,49E-07	3,45E-07	2,67E-07	3,21E-07	-0,0029

Table S2. Raw values derived from individual tumor cell lines related to figure S3F.

Table S3

Gene	rank	regulation by SIK3	reported role in tumorigenesis	reference
ST5	1	induced	suppressor	1
ELOVL7	2	induced	promotor	2
ALCAM	3	induced	promotor	3
CD83	4	induced	n.a.	
CD40	5	induced	promotor	4
MATN2	6	induced	promotor	5
PTP4A3	7	induced	promotor	6
IFIH1	8	induced	n.a.	
CNKSR3	9	induced	suppressor	7
NFATC1	10	induced	promotor	8
ANKRD33B	11	induced	n.a.	
CFAP46	12	induced	n.a.	
FMNL3	13	induced	promotor	9
MX1	14	induced	promotor	10
CCL5	15	induced	promotor	11
STAT5A	16	induced	promotor	12
GFPT2	17	induced	promotor	13
AP1S3	18	induced	promotor	14
RIPK2	19	induced	promotor	15
SLFN5	20	induced	dual	16, 17
CD69	21	induced	n.a.	
TRAF1	22	induced	promotor	18
CLIP2	23	induced	promotor	19
CSGALNACT1	24	induced	promotor	20
CRISPLD2	25	induced	n.a.	
DRAM1	26	induced	suppressor	21
SNN	27	induced	n.a.	
GATA6	28	induced	suppressor	22
TMCC2	29	induced	n.a.	
MARCKS	30	induced	promotor	23
GLRX	31	induced	promotor	24
CCL20	32	induced	promotor	25
BTN2A2	33	induced	n.a.	
RASSF5	34	induced	suppressor	26
SEMA4C	35	induced	promotor	27
NKX3-1	36	induced	suppressor	28
RNF144A	37	induced	promotor	29
STAP2	38	induced	promotor	30
GCNT4	39	induced	n.a.	
TMEM120A	40	induced	n.a.	
DOCK10	41	induced	promotor	31
FSCN1	42	induced	promotor	32
ICAM1	43	induced	promotor	33
ALS2CL	44	induced	suppressor	34
CGN	45	induced	n.a.	
RASGEF1A	46	induced	promotor	35

BCL2L11	47	induced	n.a.	
TIAM1	48	induced	promotor	36
GABBR1	49	induced	n.a.	
SP6	50	induced	n.a.	
RFX2	51	induced	suppressor	37
XAF1	52	induced	suppressor	38
EBI3	53	induced	promotor	39
SOD2	54	induced	promotor	40
AMER1	55	induced	n.a.	
CD74	56	induced	promotor	41
DHX58	57	induced	promotor	42
RPS6KA2	58	induced	promotor	43
SPNS2	59	induced	promotor	44
RAP1GAP	60	induced	suppressor	45
BARX2	61	induced	suppressor	46
SLC15A3	62	induced	n.a.	
LRRC32	63	induced	promotor	47
TMEM231	64	induced	n.a.	
GAL	65	induced	promotor	48
CITED4	66	induced	promotor	49
CD82	67	induced	suppressor	50
SAA1	68	induced	promotor	
LAD1	69	induced	n.a.	
TTC39A	70	induced	n.a.	
CTSS	71	induced	promotor	51
CYP7B1	72	induced	n.a.	
L3MBTL4	73	induced	suppressor	52
FZD9	74	induced	dual	53
SELE	75	induced	n.a.	
TNFRSF9	76	induced	dual role	54
OAS2	77	induced	n.a.	
EGR3	78	induced	n.a.	
PDLIM4	79	induced	suppressor	55
SERPINE2	80	induced	promotor	56
MYB	81	induced	promotor	57
MGLL	82	induced	promotor	58
RFTN1	83	induced	n.a.	
KCNQ4	84	induced	promotor	59
RGS3	85	induced	n.a.	
CBFA2T3	86	induced	n.a.	
IL12A	87	induced	n.a.	
CSF2	88	induced	n.a.	
RHOV	89	induced	promotor	60
WNT4	90	induced	promotor	61
HSPA12A	91	induced	n.a.	

Table S3. Induced genes related to Fig. 5B. Genes induced by SIK3 upon TNF stimulation. Rank relates to position in Fig. 5B. Role of indicated genes in tumor promotion or suppression as reported by reference. N.a; no clear role in tumor cell intrinsic biology found.

References related to Tab S3.

1. Lichy JH, Majidi M, Elbaum J, Tsai MM. Differential expression of the human ST5 gene in HeLa-fibroblast hybrid cell lines mediated by YY1 evidence that YY1: Plays a part in tumor suppression. *Nucleic Acids Res* **24**, 4700-4708 (1996).
2. Tamura K*, et al.* Novel lipogenic enzyme ELOVL7 is involved in prostate cancer growth through saturated long-chain fatty acid metabolism. *Cancer Res* **69**, 8133-8140 (2009).
3. Kahlert C*, et al.* Increased expression of ALCAM/CD166 in pancreatic cancer is an independent prognostic marker for poor survival and early tumour relapse. *Brit J Cancer* **101**, 457-464 (2009).
4. Kim H*, et al.* Direct Interaction of CD40 on Tumor Cells with CD40L on T Cells Increases the Proliferation of Tumor Cells by Enhancing TGF-beta Production and Th17 Differentiation. *Plos One* **10**, (2015).
5. Korpos E, Deak F, Kiss I. Matrilin-2, an extracellular adaptor protein, is needed for the regeneration of muscle, nerve and other tissues. *Neural Regen Res* **10**, 866-869 (2015).
6. Stephens BJ, Han HY, Gokhale V, Von Hoff DD. PRL phosphatases as potential molecular targets in cancer. *Mol Cancer Ther* **4**, 1653-1661 (2005).
7. Nie HZ*, et al.* Mineralocorticoid receptor suppresses cancer progression and the Warburg effect by modulating the miR-338-3p-PKLR axis in hepatocellular carcinoma. *Hepatology* **62**, 1145-1159 (2015).
8. Gardberg M, Heuser VD, Koskivuo I, Koivisto M, Carpen O. FMNL2/FMNL3 formins are linked with oncogenic pathways and predict melanoma outcome. *The journal of pathology Clinical research* **2**, 41-52 (2016).
9. Baumgart S*, et al.* Inflammation-induced NFATc1-STAT3 transcription complex promotes pancreatic cancer initiation by KrasG12D. *Cancer discovery* **4**, 688-701 (2014).
10. Hastie E, Cataldi M, Moerdyk-Schauwecker MJ, Felt SA, Steuerwald N, Grdzelishvili VZ. Novel biomarkers of resistance of pancreatic cancer cells to oncolytic vesicular stomatitis virus. *Oncotarget* **7**, 61601-61618 (2016).
11. Igelmann S, Neubauer HA, Ferbeyre G. STAT3 and STAT5 Activation in Solid Cancers. *Cancers (Basel)* **11**, (2019).
12. Szymura SJ*, et al.* NF-kappa B upregulates glutamine-fructose-6-phosphate transaminase 2 to promote migration in non-small cell lung cancer. *Cell Commun Signal* **17**, (2019).
13. Sung GH, Chang H, Lee JY, Song SY, Kim HS. Pancreatic-cancer-cell-derived trefoil factor 2 impairs maturation and migration of human monocyte-derived dendritic cells in vitro. *Animal cells and systems* **22**, 368-381 (2018).
14. Zare A*, et al.* RIPK2: New Elements in Modulating Inflammatory Breast Cancer Pathogenesis (vol 10, 184, 2018). *Cancers* **10**, (2018).
15. Arslan AD*, et al.* Human SLFN5 is a transcriptional co-repressor of STAT1-mediated interferon responses and promotes the malignant phenotype in glioblastoma. *Oncogene* **36**, 6006-6019 (2017).
16. Sassano A*, et al.* Human Schlafen 5 (SLFN5) Is a Regulator of Motility and Invasiveness of Renal Cell Carcinoma Cells. *Mol Cell Biol* **35**, 2684-2698 (2015).
17. Baldwin AS. Control of oncogenesis and cancer therapy resistance by the transcription factor NF-kappaB. *The Journal of clinical investigation* **107**, 241-246 (2001).

18. Kaiser JC*, et al.* Integration of a radiation biomarker into modeling of thyroid carcinogenesis and post-Chernobyl risk assessment. *Carcinogenesis* **37**, 1152-1160 (2016).
19. Afratis N*, et al.* Glycosaminoglycans: key players in cancer cell biology and treatment. *Febs J* **279**, 1177-1197 (2012).
20. Guan JJ, Zhang XD, Sun W, Qi L, Wu JC, Qin ZH. DRAM1 regulates apoptosis through increasing protein levels and lysosomal localization of BAX. *Cell Death Dis* **6**, (2015).
21. Martinelli P*, et al.* GATA6 regulates EMT and tumour dissemination, and is a marker of response to adjuvant chemotherapy in pancreatic cancer. *Gut* **66**, 1665-1676 (2017).
22. Chen CH, Fong LWR, Yu E, Wu R, Trott JF, Weiss RH. Upregulation of MARCKS in kidney cancer and its potential as a therapeutic target. *Oncogene* **36**, 3588-3598 (2017).
23. Wang LL*, et al.* GLRX inhibition enhances the effects of geftinib in EGFR-TKI-resistant NSCLC cells through FoxM1 signaling pathway. *J Cancer Res Clin* **145**, 861-872 (2019).
24. Liu BY*, et al.* Tumor-associated macrophage-derived CCL20 enhances the growth and metastasis of pancreatic cancer. *Acta Bioch Bioph Sin* **48**, 1067-1074 (2016).
25. Zhou XH, Yang CQ, Zhang CL, Gao Y, Yuan HB, Wang C. RASSF5 inhibits growth and invasion and induces apoptosis in osteosarcoma cells through activation of MST1/LATS1 signaling. *Oncol Rep* **32**, 1505-1512 (2014).
26. Kato S*, et al.* Semaphorin 4D, a lymphocyte semaphorin, enhances tumor cell motility through binding its receptor, plexinB1, in pancreatic cancer. *Cancer Sci* **102**, 2029-2037 (2011).
27. Song LN, Silva J, Koller A, Rosenthal A, Chen EI, Gelmann EP. The Tumor Suppressor NKX3.1 Is Targeted for Degradation by DYRK1B Kinase. *Mol Cancer Res* **13**, 913-922 (2015).
28. Li BY, He LJ, Zhang XL, Liu H, Liu B. High expression of RAB38 promotes malignant progression of pancreatic cancer. *Mol Med Rep* **19**, 909-918 (2019).
29. Kitai Y*, et al.* STAP-2 protein promotes prostate cancer growth by enhancing epidermal growth factor receptor stabilization. *J Biol Chem* **292**, 19392-19399 (2017).
30. Shin S*, et al.* ERK2 regulates epithelial-to-mesenchymal plasticity through DOCK10-dependent Rac1/FoxO1 activation. *Proc Natl Acad Sci U S A* **116**, 2967-2976 (2019).
31. Chen Y*, et al.* FSCN1 is an effective marker of poor prognosis and a potential therapeutic target in human tongue squamous cell carcinoma. *Cell Death Dis* **10**, (2019).
32. Lee DJ*, et al.* Multiple tumor-suppressor genes on chromosome 3p contribute to head and neck squamous cell carcinoma tumorigenesis. *Cancer Biol Ther* **10**, 689-693 (2010).
33. Ura K, Obama K, Satoh S, Sakai Y, Nakamura Y, Furukawa Y. Enhanced RASGEF1A expression is involved in the growth and migration of intrahepatic cholangiocarcinoma. *Clinical cancer research : an official journal of the American Association for Cancer Research* **12**, 6611-6616 (2006).
34. Guo X*, et al.* Balanced Tiam1-rac1 and RhoA drives proliferation and invasion of pancreatic cancer cells. *Mol Cancer Res* **11**, 230-239 (2013).
35. Liou GY*, et al.* Mutant KRAS-induced expression of ICAM-1 in pancreatic acinar cells causes attraction of macrophages to expedite the formation of precancerous lesions. *Cancer discovery* **5**, 52-63 (2015).

36. Su JC*, et al.* RFX-1-dependent activation of SHP-1 inhibits STAT3 signaling in hepatocellular carcinoma cells. *Carcinogenesis* **35**, 2807-2814 (2014).
37. Huang J*, et al.* XAF1 as a prognostic biomarker and therapeutic target in pancreatic cancer. *Cancer Sci* **101**, 559-567 (2010).
38. Huang CB*, et al.* Tumour-derived Interleukin 35 promotes pancreatic ductal adenocarcinoma cell extravasation and metastasis by inducing ICAM1 expression. *Nat Commun* **8**, (2017).
39. He C*, et al.* SOD2 acetylation on lysine 68 promotes stem cell reprogramming in breast cancer. *Proc Natl Acad Sci U S A* **116**, 23534-23541 (2019).
40. Gold DV, Stein R, Burton J, Goldenberg DM. Enhanced expression of CD74 in gastrointestinal cancers and benign tissues. *Int J Clin Exp Patho* **4**, 1-12 (2011).
41. Ranoa DRE*, et al.* Cancer therapies activate RIG-I-like receptor pathway through endogenous non-coding RNAs. *Oncotarget* **7**, 26496-26515 (2016).
42. Milosevic N*, et al.* Synthetic lethality screen identifies RPS6KA2 as modifier of epidermal growth factor receptor activity in pancreatic cancer. *Neoplasia* **15**, 1354-1362 (2013).
43. Gu XY*, et al.* SPNS2 promotes the malignancy of colorectal cancer cells via regulating Akt and ERK pathway. *Clin Exp Pharmacol P* **46**, 861-871 (2019).
44. Zhang LZ*, et al.* Identification of a putative tumor suppressor gene Rap1GAP in pancreatic cancer. *Cancer Res* **66**, 898-906 (2006).
45. Chen H*, et al.* Downregulation of BarH-like homeobox 2 promotes cell proliferation, migration and aerobic glycolysis through Wnt/-catenin signaling, and predicts a poor prognosis in non-small cell lung carcinoma. *Thorac Cancer* **9**, 390-399 (2018).
46. Tran DQ, Andersson J, Wang R, Ramsey H, Unutmaz D, Shevach EM. GARP (LRRC32) is essential for the surface expression of latent TGF-beta on platelets and activated FOXP3(+) regulatory T cells. *P Natl Acad Sci USA* **106**, 13445-13450 (2009).
47. Chetry M*, et al.* The Role of Galectins in Tumor Progression, Treatment and Prognosis of Gynecological Cancers. *Journal of Cancer* **9**, 4742-4755 (2018).
48. Hsieh CH, Chou YT, Kuo MH, Tsai HP, Chang JL, Wu CW. A targetable HB-EGF-CITED4 axis controls oncogenesis in lung cancer. *Oncogene* **36**, 2946-2956 (2017).
49. Zhu JD*, et al.* The metastasis suppressor CD82/KAI1 regulates cell migration and invasion via inhibiting TGF-beta 1/Smad signaling in renal cell carcinoma. *Oncotarget* **8**, 51559-51568 (2017).
50. Djurec M*, et al.* Saa3 is a key mediator of the protumorigenic properties of cancer-associated fibroblasts in pancreatic tumors. *P Natl Acad Sci USA* **115**, E1147-E1156 (2018).
51. Gautam J, Bae YK, Kim JA. Up-regulation of cathepsin S expression by HSP90 and 5-HT7 receptor-dependent serotonin signaling correlates with triple negativity of human breast cancer. *Breast Cancer Res Tr* **161**, 29-40 (2017).
52. Addou-Klouche L*, et al.* Loss, mutation and deregulation of L3MBTL4 in breast cancers. *Mol Cancer* **9**, (2010).
53. Zeng CM, Chen Z, Fu L. Frizzled Receptors as Potential Therapeutic Targets in Human Cancers. *Int J Mol Sci* **19**, (2018).
54. Glorieux C, Huang P. Regulation of CD137 expression through K-Ras signaling in pancreatic cancer cells. *Cancer Commun* **39**, (2019).
55. Vanaja DK*, et al.* PDLIM4, An Actin Binding Protein, Suppresses Prostate Cancer Cell Growth. *Cancer Invest* **27**, 264-272 (2009).
56. Yang Y, Xin XK, Fu X, Xu DM. Expression pattern of human SERPINE2 in a variety of human tumors. *Oncol Lett* **15**, 4523-4530 (2018).

57. Srivastava SK, *et al.* MYB is a novel regulator of pancreatic tumour growth and metastasis. *Brit J Cancer* **113**, 1694-1703 (2015).
58. Li CF, *et al.* Transcriptomic reappraisal identifies MGLL overexpression as an unfavorable prognosticator in primary gastrointestinal stromal tumors. *Oncotarget* **7**, 49986-49997 (2016).
59. Comes N, *et al.* Involvement of potassium channels in the progression of cancer to a more malignant phenotype. *Bba-Biomembranes* **1848**, 2477-2492 (2015).
60. Haga RB, Ridley AJ. Rho GTPases: Regulation and roles in cancer cell biology. *Small GTPases* **7**, 207-221 (2016).
61. Vouyovitch CM, *et al.* WNT4 mediates the autocrine effects of growth hormone in mammary carcinoma cells. *Endocrine-related cancer* **23**, 571-585 (2016).
62. Zhang H, *et al.* LAMB3 mediates apoptotic, proliferative, invasive, and metastatic behaviors in pancreatic cancer by regulating the PI3K/Akt signaling pathway. *Cell Death Dis* **10**, (2019).
63. Li H, *et al.* C1QTNF1-AS1 regulates the occurrence and development of hepatocellular carcinoma by regulating miR-221-3p/SOCS3. *Hepatology international* **13**, 277-292 (2019).
64. Liu N, Gao F, Han Z, Xu X, Underhill CB, Zhang L. Hyaluronan synthase 3 overexpression promotes the growth of TSU prostate cancer cells. *Cancer Res* **61**, 5207-5214 (2001).

Table S4

Gene	rank	regulation by SIK3	reported role in tumorigenesis	Reference
ANGPTL4	1	repressed	suppressor	1
ID2	2	repressed	promotor	2
INTS6	3	repressed	suppressor	3
SPRY1	4	repressed	suppressor	4
TOB1	5	repressed	suppressor	5
EID3	6	repressed	suppressor	6
KCNQ1OT1	7	repressed	suppressor	7
GNAI1	8	repressed	suppressor	8
HES1	9	repressed	suppressor	9
HIST4H4	10	repressed	n.a.	
HTR1B	11	repressed	suppressor	10
MEG3	12	repressed	suppressor	11
FOXQ1	13	repressed	promotor	12
DMRTA1	14	repressed	n.a.	
SNAI1	15	repressed	promotor	13
SNORD17	16	repressed	n.a.	
GRIP1	17	repressed	n.a.	
CALCRL	18	repressed	n.a.	

Table S4. Repressed genes; related to Fig. 5B. Genes repressed by SIK3 upon TNF stimulation. Rank relates to position in Fig. 5B. Role of indicated genes in tumor promotion or suppression as reported by reference. N.a; no clear role in tumor cell intrinsic biology found.

References related to Tab S4.

1. Coma S, Amin DN, Shimizu A, Lasorella A, Iavarone A, Klagsbrun M. Id2 Promotes Tumor Cell Migration and Invasion through Transcriptional Repression of Semaphorin 3F. *Cancer Res* **70**, 3823-3832 (2010).
2. Filleur S*, et al.* INTS6/DICE1 inhibits growth of human androgen-independent prostate cancer cells by altering the cell cycle profile and Wnt signaling. *Cancer Cell Int* **9**, (2009).
3. Hidalgo-Sastre A*, et al.* Hes1 Controls Exocrine Cell Plasticity and Restricts Development of Pancreatic Ductal Adenocarcinoma in a Mouse Model. *Am J Pathol* **186**, 2934-2944 (2016).
4. Lee HS, Kundu J, Kim RN, Shin YK. Transducer of ERBB2.1 (TOB1) as a Tumor Suppressor: A Mechanistic Perspective. *Int J Mol Sci* **16**, 29815-29828 (2015).
5. Liu JY, Wu XY, Wu GN, Liu FK, Yao XQ. FOXQ1 promotes cancer metastasis by PI3K/AKT signaling regulation in colorectal carcinoma. *Am J Transl Res* **9**, 2207-+ (2017).
6. Ma L*, et al.* Long non-coding RNA MEG3 functions as a tumour suppressor and has prognostic predictive value in human pancreatic cancer. *Oncol Rep* **39**, 1132-1140 (2018).
7. Masoumi-Moghaddam S, Amini A, Morris DL. The developing story of Sprouty and cancer. *Cancer Metast Rev* **33**, 695-720 (2014).
8. Okochi-Takada E*, et al.* ANGPTL4 is a secreted tumor suppressor that inhibits angiogenesis. *Oncogene* **33**, 2273-2278 (2014).
9. Shuno Y*, et al.* Id1/Id3 Knockdown Inhibits Metastatic Potential of Pancreatic Cancer. *J Surg Res* **161**, 76-82 (2010).
10. Sun X*, et al.* Overexpression of long non-coding RNA KCNQ1OT1 is related to good prognosis via inhibiting cell proliferation in non-small cell lung cancer. *Thorac Cancer* **9**, 523-531 (2018).
11. Takai D*, et al.* Silencing of HTR1B and reduced expression of EDN1 in human lung cancers, revealed by methylation-sensitive representational difference analysis. *Oncogene* **20**, 7505-7513 (2001).
12. Yao J*, et al.* GNAI1 Suppresses Tumor Cell Migration and Invasion and is Post-Transcriptionally Regulated by Mir-320a/c/d in Hepatocellular Carcinoma. *Cancer biology & medicine* **9**, 234-241 (2012).
13. Yin T, Wang CY, Liu T, Zhao G, Zha YH, Yang M. Expression of snail in pancreatic cancer promotes metastasis and chemoresistance. *J Surg Res* **141**, 196-203 (2007).

Supplementary Material and Methods

^{51}Chromium-release assay

Tumor cells were detached and labelled with 100 µL 51Cr/106 target cells in CLM for 1 h at 37 °C. Afterwards, cells were washed with CLM and incubated with PBS-EDTA (1:20 dilution; Merck Millipore) at 37°C for 10 minutes. Tumor cells were counted and 3000 target cells per well were co-cultured with T cells in 96 well u-bottom plates at the indicated E:T

ratios for 6 h at 37°C. Plates were centrifuged and 100 µL of supernatants were collected in 96-well Luma plates (Perkin Elmer, Waltham USA). Plates were dried overnight, and radioactivity counted in the Gamma counter (Cobra counter Packard, Perkin Elmer). Spontaneous release was measured from the target cells that are incubated with medium alone, whereas maximum release was determined from the target cells incubated with 10% Triton X-100 (Merck Millipore) instead of T cells. The percent of specific lysis was calculated by using the formula given below: % Specific lysis = (experimental release-spontaneous release) / (maximum release-spontaneous release) × 100.

Influenza-specific CD8+ T cells

For the generation of influenza (Flu)-specific CD8+ T (FluT) cells, PBMCs from HLA-A*02+ healthy donors were isolated. Total CD8+ T cells were sorted from PBMCs by magnetic separation and expanded in the presence of A2-matched Flu peptide (GILGFVFTL, ProImmune, Oxford, UK) for 14 days. The autologous CD8- fraction was irradiated and used for 1 week as feeder cells, which were then substituted with irradiated T2 cells. On day 1 and day 8, 100 U/ml IL2 and 5 ng/µL IL15 were added. Cells were expanded in expansion medium composed of 50% CLM and 50% AIM-V medium. After 14 days of antigen-specific expansion, pentamer-labelled Flu-antigen specific T cells were sorted by FACS and expanded further for 14 days according to the rapid expansion protocol from Rosenberg *et al.* [1].

Western blot

Tumor cells were centrifuged and cell pellets resuspended in lysis buffer (MILLIPLEX MAP Lysis Buffer from Merck Millipore, protease inhibitor cocktail (Merck Millipore) and phosphatase inhibitor cocktail (Sigma-Aldrich)) and kept on ice for 15 min. After mixture, whole cell lysate was cleared by centrifugation (10 min, 10000g, 4 °C). For cytosolic and nuclear extraction cell pellets were resuspended in 5 cell pellet volumes ice cold Buffer A (10 mM HEPES (pH 7.9), 1.5 mM MgCl2, 10 mM KCl, 1 mM DTT, 0.1% Triton X-100 and

Protease and Phosphatase Inhibitor Cocktail). After 10 min incubation cell suspension was centrifuged (300 g, 5 min, 4°C), supernatant discarded and pellet thoroughly resuspended in two volumes of Buffer A. After a centrifugation step (8000 g, 20 min, 4°C) the supernatant was collected containing cytoplasmic proteins. The remaining pellet was lysed with 2/3 of the original pellet volume ice cold Buffer B (20 mM HEPES (pH 7.9), 1.5 mM MgCl2, 0.42 M NaCl, 0.2 mM EDTA, 1 mM DTT, 1.0% NP-40, 25% (v/v) glycerol, Protease and Phosphatase Inhibitor Cocktail). Nuclear extract was collected after 45 min incubation at 4°C using a rotator and centrifugation (16000g, 5 min, 4°C). The protein content in the lysate was measured by using Pierce BCA Protein Assay Kit (Thermo Scientific) according to manufacturer's protocol. For immunoblot analysis, 30–50 µg of total protein were denatured in NuPAGE LDS Sample Buffer (Thermo Scientific) at 70°C for 10 min and separated on the NuPAGE 4-12% Bis-Tris Gels (Thermo Scientific). Separated protein bands were transferred onto PVDF membrane (Merck Millipore) using 1X wet-transfer buffer at 400 mA for 1 h at 4°C. Membranes were blocked with 5% milk powder in TBS at room temperature (RT) for 1-2 h. For the detection of phosphorylated proteins, membranes were blocked with 5% BSA in TBS-T. Membranes were incubated overnight at 4°C with the indicated primary antibodies. The following antibodies were purchased from Cell Signaling and used at 1:1000 dilution: rabbit monoclonal anti-A20/TNFAIP3 (D13H3, Cat.#5630), rabbit monoclonal anti-c-IPA2/BIRC3 (58C7,Cat.#3130), rabbit monoclonal anti-XIAP (3B6, Cat.#2045), rabbit monoclonal anti-Bcl-xL/BCL2L1 (54H6, Cat.#2764), rabbit monoclonal anti-Mcl-1 (D2W9E, Cat.#94296), rabbit monoclonal anti-CFLAR/FLIP (D5J1E, Cat.#56343), rabbit polyclonal anti-IKKβ (L570, Cat.#2678), rabbit polyclonal anti-IKKα (Cat.#2682), rabbit monoclonal anti-phospho-IKKα/β (Ser176/180) (16A6, Cat.#2697), rabbit monoclonal anti-IκBα (44D4, Cat.#4812), rabbit monoclonal anti-phospho-IκBα (Ser32) (14D4, Cat.#2859), rabbit monoclonal anti-LKB1 (27D10, Cat.#3050), rabbit monoclonal anti-phospho-LKB1 (Ser428) (C67A3,

Cat.#3482), anti-HDAC4, anti-pHDAC4 (Ser246), anti-NF-κB and polyclonal anti-acNF-κB (Lys310) and anti-Histone H3. As housekeeper gene, mouse monoclonal anti-GAPDH (0411, Cat.#sc-47724) was purchased from Santa Cruz and used 1:200. Rabbit polyclonal anti-SIK3 was purchased from Abcam, Cat.#88495 and used 1:1000. Membranes were washed 3 times with TBS-T for 10 min and incubated 1 h at room temperature with HRP-conjugated secondary antibodies (anti-mouse and anti-rabbit, Santa Cruz, Dallas, USA) prepared in 1% milk in TBS-T or in 5% BSA in TBS-T for the detection of phosphorylated proteins. Protein bands were detected using ECL developing solution from GE Healthcare and the chemiluminescent signal was detected using the My ECL Imager (Thermo Scientific).

PCR and qPCR

Synthesized cDNA was amplified using conventional PCR. PCR samples were set up in a 25 µL volume using 2x MyTaq HS Red Mix (Bioline, Luckenwalde, Germany), 500 nM of gene-specific primer mix (Qiagen, Hilden, Germany) and 100 ng of template cDNA. The PCR program was set as follows: 95°C for 3 min, 35 cycles of a 3 repetitive steps of denaturation (95°C for 15 s), annealing (60°C for 20 s) and extension (72°C for 15 s), and a final step at 72°C for 7 min. PCR products were run on a 2% agarose gel and visualized using a UV documentation system (Konrad Benda, Wiesloch, Germany). For qPCR, 10 ng of template cDNA, 2x QuantiFast SYBR Green PCR mix (Qiagen) and 300 nM of gene-specific primer mix was used per 20 µL reaction. Reactions were run using the 7300 Real-Time PCR System (Thermo Scientific, Waltham, Massachusetts, USA). The following primers were used for cDNA detection: RT2 qPCR Primer Assay for Human MCL1 (QIAGEN PPH00397E-200); RT2 qPCR Primer Assay for Human XIAP (QIAGEN PPH00323A-200); RT² qPCR Primer Assay for Human SIK3 (QIAGEN PPH21242A-200); RT2 qPCR Primer Assay for Human BIRC3 (cIAP2) (QIAGEN PPH00326B-200); RT2 qPCR Primer Assay for Human CFLAR (QIAGEN PPH00333B-200); RT2 qPCR Primer Assay for Human TNFAIP3 (A20) (QIAGEN

PPH00063A-200). Expression of analyzed genes was normalized to the expression of β-actin (Fwd: AGAAAATCTGGCACCACACC; Rvs: GGGGTGTTGAAGGTCTCAAA) or GAPDH (QIAGEN PPH00150F-200) genes and the analysis was performed using comparative Ct method.

Gene overexpression

For SIK3 overexpression 3 x 10^5 M579 cells or 2 x 10^6 PANC-1 cells were seeded in a 6-well plate overnight at 37°C, 5% CO2. 3 µg of SIK3-overexpression plasmid (GenScript, Piscataway USA) or the empty vector (EV) control (pCDNA3.1; GenScript) were diluted in 150 µL of Opti-MEM (Thermo Scientific) in the presence of 3 µL of the plus reagent. 15 µL of Lipofectamine LTX (Thermo Scientific) was suspended in 150 µL of Opti-MEM. The DNA-containing solution was added to the liposome-containing suspension and incubated for 30 min at RT. The tumor cell medium was replaced with 1 ml of Opti-MEM and the DNA-liposome mixture was added dropwise to the tumor cells. After 24 h the tumor cell medium was replaced with normal cell culture medium. PANC-1- luc cells overexpressing the anti-apoptotic genes (A20 (NM_001270508.2), cIAP2 (NM_001165.5), cFLIP (NM_003879.7), XIAP (NM_001167.3) and MCL-1 (NM_021960.5)) were generated by stable transfection. PANC-1-luc cell line was transfected with the ORF for each gene, cloned in pcDNA3.1/Hygro(+) vectors, obtained from GenScript (Clone IDs: OHu14590, OHu18994,OHu23686, OHu20683, OHu21277 respectively), using jetOptimus (PolyPlus, cat.#. 101000051), according to manufacturer's instructions. The transfected cells were selected with 500 µg/ml Hygromycin B (Carl-Roth, cat.# 1287.2).

ELISA

siRNA-transfected PANC-1 or M579 cells were co-cultured with different T cell sources at the indicated E:T ratio for 20 h and 100 µL of supernatants were harvested for the detection of IFN γ (Human IFN-γ ELISA Set; BD OptEIA™; Heidelberg, Germany), perforin (Human Perforin

ELISA PRO kit, Mabtech, Nacka Strand, Sweden) and granzyme B (Human Granzyme B ELISA development kit; Mabtech). Experiments were performed according to the manufacturer´s instructions. PMA/Ionomycin (Merck Millipore; 50 ng/ml and 1 µg/ml final concentration respectively) stimulation was used as a positive control. Absorbance was measured at $\lambda = 450$ nm, taking $\lambda = 570$ nm as reference wavelength using a microplate reader (TECAN, Männedorf, Switzerland).

Flow cytometry

For flow cytometry experiments, live cells were distinguished by using Live/Dead Fixable Yellow dead Cell Stain (Life Technologies) followed by blocking with kiovig (human plasma-derived immunoglobulin, Baxter, Deerfield, Illinois, USA) at a concentration of 100 µg/ml in FACS buffer (PBS, 2% FCS) for 15 min at 4°C. Samples were washed in FACS buffer and incubated with either fluorophore-conjugated primary antibody or isotype control (anti-PD1; Biolegend, San Diego, USA 1:20, anti-TIM-3 and anti-LAG3; both R&D Systems, Miniapolis, USA 1:20). Cells were acquired with the FACS Canto II cell analyzer machine (BD). For indirect flow cytometry (TNFR-I (Hycult biotech) or TNFR-II (Acris antibodies) stainings) samples were incubated with the primary antibody and subsequently stained with phycoerythrin (PE)-conjugated secondary antibody 1:4000 (Jackson Immuno) for 20 min on ice in the dark. For assessing tumor cell proliferation, 50000 M579 tumor cells or PANC-1 tumor cells labeled with 0.5µM CFSE (eBioscience) were plated in 6 well plates and left to adhere. After 3-4 h, TIL209 or TIL412 (in CLM medium) were added to M579 cells at varying E:T ratios. Similarly, TILs or FluT cells (in CLM medium) were added to PANC-1 tumor cells. PANC-1 cells were previously pulsed with Flu peptide for 2h in the wells where FluT cells were to be added. 24 h later, cells were disrupted using trypsin EDTA (Lonza) and live cells were distinguished by using the Live/Dead Fixable Yellow dead Cell Stain followed by blocking with kiovig and stained for EpCAM or the corresponding isotype control antibody

(Biolegend) for 20 min at 4°C. Cells were then fixed and permeabilized using fixation and permeabilization concentrate and diluent from eBioscience for 20 min at 4 °C followed by intracellular staining for Ki67 (BD Biosciences) in 1x permeabilization solution (eBioscience) for 20 min at 4 °C. Acquisition of cells were performed using the BD LSRII, and data analysis was done with FlowJo V10 software. EpCAM positive PANC-1 cells were analyzed for Ki67 expression. CFSE-stained M579 cells were analysed for Ki67 expression.

TNF-α catch assay

1 x 10^6 TILs cells were co-cultured with 1 x 10^6 PANC-1 WT cells (E:T = 1:1) in a 12-well plate. Alternatively, TILs were polyclonally stimulated with PHA (5 µg/ml final concentration; Merck Millipore). Unstimulated T cells served as negative control. After 12h incubation, T cells were collected and stained with the TNF secretion assay (catch assay) kit (Miltenyi biotech, Bergisch Gladbach, Germany) according to manufacturer´s instructions. Briefly, TILs were collected and incubated with the cytokine catch reagent for 5 min on ice. Afterwards, warm medium was added and cells were incubated for 1 h at 37°C, 5% CO2. Catch reagent was washed out and the cytokine detection antibody (PE-conjugated) was added together with anti-CD3, anti-CD4 and anti-CD8 antibodies in the presence of Live/Dead Fixable Yellow dead Cell Stain (1:1000). After 20 min incubation on ice in the dark TILs were washed twice and measured via FACS.

NF-κB reporter assay

TNF-induced NF-κB activity in PANC-1 cells was measured using NF-κB-dependent luciferase activity. NF-κB reporter PANC-1 cells (carrying the luciferase gene under the control of NF-κB promoter) were seeded in 96 or 384-well plates for 24 h (experiment with inhibitors) or 72h (experiment with siRNAs) Afterwards, cells were treated with different concentrations of the SIK3 inhibitor HG-9-91-01 for one hour before addition of 10 ng/ml rHu

TNF for 7h at 37°C and 5% CO_2. For siRNA-based assays, 100 ng/mL of rHuTNF was used for 24h. Afterwards, cells were lysed, and luciferase activity was measured.

pHDAC4 MSD assay

HDAC4 phosphorylation levels in PANC-1 cells were measured using a Meso Scale Discovery assay. PANC-1 cells (6 x 1010^4) were seeded in a 96-well plate overnight and subsequently treated with 10 ng/mL rHu TNF and different concentrations of the SIK3 inhibitor HG-9-91-01 for 3 h at 37°C and 5% CO_2. Whole cell lysates were generated using RIPA lysis buffer (Thermo Scientific) and incubated on GAM plates coated with anti-total HDAC4 antibody (Abcam ab12171) overnight at 4 °C. Afterwards, phosphorylated HDAC4 was detected using the pHDAC4 antibody (CST#3443). ECL signal was measured using an MSD reader.

Luminex assays

TNF was quantified using BioPlex ProHuman Chemokine TNFa Set (Bio-Rad) according to the manufacturer´s instructions. Samples were measured using the MAGPIX luminex instrument (Merck Millipore). For detection of intracellular analytes involved in apoptosis PANC-1 cells were stimulated with rHuTNF (100 ng/ml) for 2h or 4 h, lysed and 20 µg of protein lysates were used for detection of phosphorylated Akt (Ser473), JNK (Thr183/Tyr185), Bad (Ser112), Bcl-2 (Ser70), p53 (Ser46) or cleaved Caspase-8 (Asp384) and Caspase-9 (Asp315) by MILLIPLEX MAP Early Phase Apoptosis 7-plex-kit (Millipore) according to the manufacturer´s instructions. Samples were measured using the MAGPIX luminex instrument (Merck Millipore).

Real-time live cell imaging

Transfected tumor cells were challenged either with T cells or with 100 ng/ml of rHuTNF. Alternatively, 1 x 10^5 M579 were seeded in a 96-well plate flat overnight and subsequently challenged with TIL209 (5:1). In some experiments, TILs were labelled with Cell Trace Far Red (Cell Trace Proliferation Kit from Thermo Scientific) prior to co-culture. All reactions

were conducted in the presence of the YOYO-1 dye (Thermo Scientific), (1:1000). Plates were incubated in the Incucyte ZOOM live-cell imager (Essen Bioscience, Welwyn Garden City, UK) at 37°C and 5% CO_2 and images were acquired at the indicated time points. Data were analyzed with the Incucyte ZOOM 2016A software (Essen Bioscience) by creating a top-hat filter-based mask for the calculation the area of YOYO-1 incorporating cells (dead cells).

WST-1 assay

The WST-1 Cell Proliferation Assay (Roche, Basel, Switzerland) was used to measure viability of PANC-1. In short, PANC-1 cells were reverse transfected and 10 µL of the WST-1 reagent was added to each well and incubated for 1h at 37°C, 5% CO_2. The absorbance was measured at $\lambda = 450$ nm versus $\lambda = 650$ nm reference by using the Spark microplate reader (TECAN). In some cases, reverse transfected cells were stimulated with the supernatant of polyclonally stimulated T cells for 24h before the addition of the WST-1 reagent.

TNF sensitization assay

TNF sensitization was measured in a screening of 94 different solid cancer cell lines (Oncolead, Munich, Germany). In short, cell lines were seeded (varying media, seeding density btw. 500 – 7000 cells/well) in a 96-well plate for 48 h at 37°C and 5% CO_2. Afterwards, cells were treated with different concentrations of HG-9-91-01 (1, 4, 16, 64, 250 and 1000 nM) and 2 ng/ml rHu TNF for 120 h at 37°C and 5% CO_2. Cytotoxicity was measured using sulforhodamine B as described before. Plate normalization was performed on all values by subtracting the background value (average optical density of wells with medium but without cells). Dose response curves were calculated using non-linear curve fitting. IC_{50} and growth inhibition of 50 % (GI_{50}) were calculated and log10-transformed. Synergy between HG-9-91-01 and TNF treatment was calculated by the highest single agent model.

ELISA

The NF-κB p50/p65 EZ-TFA Transcription Factor assay kit (Merck Millipore) was used to measure the nuclear translocation of the p65 subunit of the NF-κB complex. Briefly, PANC-1 WT or Hela cells were reverse transfected with desired siRNAs. Tumor cells were then stimulated either with 100 ng/ml of rHuTNF or with CLM for 15 or 30 min. Alternatively, PANC-1 WT cells were transfected with SIK3 overexpressing plasmid or EV (GenScript). The cytosolic protein fraction was separated from the nuclear protein fraction according to the manufacturer`s protocol. The protein concentration of nuclear fractions was determined using the BCA kit (Thermo Scientific) according to the manufacturer's protocol. 4.5 µg of nuclear lysate were added in each well of the pre-coated NF-κB (p65 subunit) ELISA 96-well plate. The assay was performed according to the manufacturer´s instructions and absorbance was measured at $\lambda = 450$ nm, taking $\lambda = 570$ nm as reference wavelength using the Spark microplate reader (TECAN).

Pre-processing and analysis of ATAC-seq data

ATAC-seq reads were trimmed using Skewer [2] and aligned to the hg38 assembly of the human genome using Bowtie2 [3] with the '-very-sensitive' parameter and a maximum fragment length of 2,000. Duplicate and unpaired reads were removed using the sambamba[4] 'markdup' command, and reads with mapping quality >30 and alignment to the nuclear genome were kept. All downstream analyses were performed on these filtered reads. For visualization purposes only, coverage files from filtered bam files were produced using bedtools genomeCoverageBed command [5]. Each position was normalized by dividing to the total library size and multiplying by 10^6, followed by conversion to a bigwig using the bedGraphToBigWig command from the UCSC genome browser tools.

Bioinformatics analysis of chromatin accessibility data

Peak calling was performed using HOMER [6] with the following approach: Two different peak sets were called, once we used the options "-style factor -fragmentLength 150 -size 350 -minDist 350 -L 4 -fdr 0.001 -tbp 1" parameters, to identify highly robust small regions of open chromatin, and in a second approach we used the parameters "-region -fragmentLength 150 -size 150 -minDist 350 -L 4 -fdr 0.001 -tbp 1" to identify larger regions of open chromatin. The two peak sets were then intersected using the bedtools intersect command with the "-u" option to create the peak set that was used for downstream analysis. For the analysis of sample sets we always created a consensus region set by merging the called peaks from all involved samples using bedtools, and we quantified the accessibility of each region in each sample by counting the number of reads from the filtered BAM file that overlapped each region. Peaks overlapping blacklisted features as defined by the ENCODE project [7] were discarded.

To normalize the chromatin accessibility signal across samples, we performed quantile normalization followed by GC content normalization by regression using the cqn R package [8]. Principal component analysis was performed with the scikit-learn library (sklearn.decomposition.PCA) applied to the chromatin accessibility values for the merged peaks across all samples in the respective sample sets. DESeq2 [9] was used on the raw count values for each sample and regulatory element to identify differential chromatin accessibility between samples. Significant regions were defined as having an FDR-corrected p-value below 0.05, an absolute $\log_2$fold change above 1, and a mean accessibility equal or greater than 10.

Motif enrichment analysis was done using HOMER [6] with the function findMotifsGenome using "-size 500 -len 8,10,12 -h" parameters. Motifs from analyses were combined to a merged motif file and filtered for redundant motifs using HOMER's compareMotifs function with the parameters "-reduceThresh 0.6 -matchThresh 10 -info 0.6 -pvalue 1e-25" and were compared to the vertebrate known motifs from the HOMER database. The enrichment of this reduced

motif set was then calculated in the peaks of the respective comparisons using the annotatePeaks function. Histograms of reads around transcription factor binding motifs were generated using HOMER by centering the peaks of interest on the investigated motifs using the annotatePeaks function, followed by counting reads from individual experiments at single base pair resolution in a radius of 1000 bp (or 150 bp) around the peak centers using the annotatePeaks function with the parameters "-hist -fragLength 1". For these histograms, all reads aligning to the + strand were offset by +4 bp, and all reads aligning to the – strand were offset −5 bp to represent the center of the transposon binding event as described previously[10]. Shifted reads were then converted in tag directories using HOMER, merged for replicate samples, and used as input for the annotatePeaks function.

Peaks were assigned to their nearest TSS using the HOMER promoter annotation. Enrichment of genes associated with regulatory elements (annotated with the nearest transcription start site) was performed thorough the Enrichr API [11] for the KEGG 2016 dataset.

References to Supplementary Materials and Methods

1. Jin J, et al. Simplified method of the growth of human tumor infiltrating lymphocytes in gas-permeable flasks to numbers needed for patient treatment. J Immunother **35**, 283-292 (2012).

2. Jiang H, Lei R, Ding SW, Zhu S. Skewer: a fast and accurate adapter trimmer for next-generation sequencing paired-end reads. BMC Bioinformatics **15**, 182 (2014).

3. Langmead B, Salzberg SL. Fast gapped-read alignment with Bowtie 2. Nat Methods **9**, 357-359 (2012).

4. Tarasov A, Vilella AJ, Cuppen E, Nijman IJ, Prins P. Sambamba: fast processing of NGS alignment formats. Bioinformatics **31**, 2032-2034 (2015).

5. Quinlan AR, Hall IM. BEDTools: a flexible suite of utilities for comparing genomic features. Bioinformatics **26**, 841-842 (2010).

6. Heinz S, et al. Simple combinations of lineage-determining transcription factors prime cis-regulatory elements required for macrophage and B cell identities. Mol Cell **38**, 576-589 (2010).

7. Consortium EP. An integrated encyclopedia of DNA elements in the human genome. Nature **489**, 57-74 (2012).

8. Hansen KD, Irizarry RA, Wu Z. Removing technical variability in RNA-seq data using conditional quantile normalization. Biostatistics **13**, 204-216 (2012).

9. Love MI, Huber W, Anders S. Moderated estimation of fold change and dispersion for RNA-seq data with DESeq2. Genome Biol **15**, 550 (2014).

10. Buenrostro JD, Giresi PG, Zaba LC, Chang HY, Greenleaf WJ. Transposition of native chromatin for fast and sensitive epigenomic profiling of open chromatin, DNA-binding proteins and nucleosome position. Nat Methods **10**, 1213-1218 (2013).

11. Kuleshov MV, et al. Enrichr: a comprehensive gene set enrichment analysis web server 2016 update. Nucleic Acids Res **44**, W90-97 (2016).